REPORT DOCUMENTATION PAGE

Form Approved OMB NO. 0704-0188

1. REPORT DATE (DD-MM-YYYY)	2. REPORT TYPE	3. DATES COVERED (From - To)
28-05-2014	Final Report	1-Oct-2011 - 31-Dec-2012

4. TITLE AND SUBTITLE	5a. CONTRACT NUMBER
Photon-Limited Information in High Resolution Laser Ranging Final Report	W911NF-11-1-0540
	5b. GRANT NUMBER
	5c. PROGRAM ELEMENT NUMBER
	1D10BQ

6. AUTHORS	5d. PROJECT NUMBER
Dr. Zeb Barber, Dr. Baris Erkmen, Jason Dahl, Tia Sharpe	
	5e. TASK NUMBER
	5f. WORK UNIT NUMBER

7. PERFORMING ORGANIZATION NAMES AND ADDRESSES	8. PERFORMING ORGANIZATION REPORT NUMBER
Montana State University 309 Montana Hall Box 172470 Bozeman, MT 59717 -2470	

9. SPONSORING/MONITORING AGENCY NAME(S) AND ADDRESS (ES)	10. SPONSOR/MONITOR'S ACRONYM(S)
U.S. Army Research Office P.O. Box 12211 Research Triangle Park, NC 27709-2211	ARO
	11. SPONSOR/MONITOR'S REPORT NUMBER(S)
	61101-PH-DRP.2

12. DISTRIBUTION AVAILIBILITY STATEMENT

Approved for Public Release; Distribution Unlimited

13. SUPPLEMENTARY NOTES

The views, opinions and/or findings contained in this report are those of the author(s) and should not contrued as an official Department of the Army position, policy or decision, unless so designated by other documentation.

14. ABSTRACT
This project is an effort under the Information in a Photon (InPho) program at DARPA\DSO. Its purpose is to investigate experimentally and theoretically the fundamental physical and information theoretic limits to laser ranging and imaging using bits of information per received photon (bpp) as a metric. This project emphasizes the use of non-brief-pulse transmit waveforms and in particular Frequency Modulated Continuous Wave (FMCW) ladar based on active linearization of tunable laser chirp sources developed by MSU-Spectrum Lab, Synthetic Aperture Ladar 2D imaging with same source, and compressive laser ranging and imaging techniques.

15. SUBJECT TERMS

laser ranging, lidar, ladar, information theory, quantum optics

16. SECURITY CLASSIFICATION OF:			17. LIMITATION OF ABSTRACT	15. NUMBER OF PAGES	19a. NAME OF RESPONSIBLE PERSON
a. REPORT	b. ABSTRACT	c. THIS PAGE	UU		Zeb Barber
UU	UU	UU			19b. TELEPHONE NUMBER
					406-994-5925

<div align="center">

Report Title

</div>

Photon-Limited Information in High Resolution Laser Ranging Final Report

<div align="center">

ABSTRACT

</div>

This project is an effort under the Information in a Photon (InPho) program at DARPA\DSO. Its purpose is to investigate experimentally and theoretically the fundamental physical and information theoretic limits to laser ranging and imaging using bits of information per received photon (bpp) as a metric. This project emphasizes the use of non-brief-pulse transmit waveforms and in particular Frequency Modulated Continuous Wave (FMCW) ladar based on active linearization of tunable laser chirp sources developed by MSU-Spectrum Lab, Synthetic Aperture Ladar 2D imaging with same source, and compressive laser ranging and imaging techniques.   Additionally, this project investigated the use of quantum mechanically entangled biphotons in the form of down converted chirp photons for ranging. Experimental activities have included: Demonstration of a compressive ranging technique that utilizes pseudorandom waveforms to sense a sparse range scene with few measurements. Extensive collection of FMCW ladar data with a strong and weak local oscillator (LO) powers showing excellent agreement with theoretical statistics and information theoretic calculations. Demonstration of quantum optical fourth order interference from a Type II KTP waveguide Spontaneous Parametric Down Conversion (SPDC) source. Demonstration of single pixel imaging with pseudo-random projected waveforms at 1500 nm and detection with single photon counting InGaAs avalalanche photodiodes. Theoretical assistance was provided in first half of the project by Dr. Baris Erkmen of JPL who was funded through a separate channel.

Enter List of papers submitted or published that acknowledge ARO support from the start of the project to the date of this printing. List the papers, including journal references, in the following categories:

<div align="center">

(a) Papers published in peer-reviewed journals (N/A for none)

</div>

Received		Paper
01/09/2013	1.00	Baris I Erkmen, Zeb W Barber, Jason R Dahl. Maximum-likelihood estimation forfrequency-modulated continuous-wave laser rangingusing photon-counting detectors, Applied Optics, (01 2013): 0. doi:
08/15/2013	3.00	Zeb W. Barber, Jason R. Dahl, Tia L. Sharpe, Baris I. Erkmen. Shot noise statistics and information theory of sensitivity limits in frequency-modulated continuous-wave ladar, Journal of the Optical Society of America A, (06 2013): 1335. doi: 10.1364/JOSAA.30.001335
08/15/2013	4.00	Baris I. Erkmen, Zeb W. Barber, Jason Dahl. Maximum-likelihood estimation for frequency-modulated continuous-wave laser ranging using photon-counting detectors, Applied Optics, (03 2013): 2008. doi: 10.1364/AO.52.002008
TOTAL:	**3**	

Number of Papers published in peer-reviewed journals:

<div align="center">

(b) Papers published in non-peer-reviewed journals (N/A for none)

</div>

Received	Paper

TOTAL:

Number of Papers published in non peer-reviewed journals:

(c) Presentations

Presentation at the DARPA\DSO InPho Program Review San Diego, CA October 4th 2012
Presentation at Annual MSU OpTec Conference Bozeman, MT August 15th 2013
Presentation at the DARPA\DSO InPho Program Review Arlington, VA November 6th 2013

Number of Presentations: 3.00

Non Peer-Reviewed Conference Proceeding publications (other than abstracts):

<u>Received</u>   <u>Paper</u>

05/28/2014 7.00 Pushkar Pandit, Jason Dahl, Zeb Barber, W. Randall Babbitt. Multi-target compressive laser ranging,
SPIE DSS. 06-MAY-14, . : ,

TOTAL: **1**

Number of Non Peer-Reviewed Conference Proceeding publications (other than abstracts):

Peer-Reviewed Conference Proceeding publications (other than abstracts):

<u>Received</u>   <u>Paper</u>

05/28/2014 6.00 Zeb Barber, Jason Dahl. Sensitivity in Synthetic Aperture Ladar Imaging,
Conference on Lasers and Electro-Optics 2014. 08-JUN-14, . : ,

08/15/2013 5.00 Baris Erkmen, Jason R. Dahl, Zeb W. Barber. Performance Analysis for FMCW Ranging Using Photon-
Counting Detectors,
CLEO: Science and Innovations. 11-JUN-13, San Jose, California. : ,

TOTAL: **2**

Number of Peer-Reviewed Conference Proceeding publications (other than abstracts):

(d) Manuscripts

Received   Paper

05/28/2014 8.00 Zeb Barber, Jason Dahl. Synthetic aperture ladar imaging demonstrations and information at very low
return levels,
Applied Optics (06 2014)

      TOTAL: **1**

Number of Manuscripts:

Books

Received   Paper

      TOTAL:

Patents Submitted

Patents Awarded

Awards

None

Graduate Students

NAME	PERCENT_SUPPORTED	Discipline
Pushkar Pandit	0.05	
Ana Baselga	0.15	
FTE Equivalent:	**0.20**	
Total Number:	**2**	

Names of Post Doctorates

NAME	PERCENT_SUPPORTED
FTE Equivalent:	
Total Number:	

Names of Faculty Supported

NAME	PERCENT_SUPPORTED	National Academy Member
Dr. Zeb Barber	0.27	
Prof. Randy Babbitt	0.04	
FTE Equivalent:	**0.31**	
Total Number:	**2**	

Names of Under Graduate students supported

NAME	PERCENT_SUPPORTED	Discipline
Pushkar Pandit	0.05	Electrical and Computer Engineering
FTE Equivalent:	**0.05**	
Total Number:	**1**	

Student Metrics
This section only applies to graduating undergraduates supported by this agreement in this reporting period

The number of undergraduates funded by this agreement who graduated during this period: 1.00

The number of undergraduates funded by this agreement who graduated during this period with a degree in science, mathematics, engineering, or technology fields:...... 1.00

The number of undergraduates funded by your agreement who graduated during this period and will continue to pursue a graduate or Ph.D. degree in science, mathematics, engineering, or technology fields:...... 1.00

Number of graduating undergraduates who achieved a 3.5 GPA to 4.0 (4.0 max scale):...... 1.00

Number of graduating undergraduates funded by a DoD funded Center of Excellence grant for Education, Research and Engineering:...... 0.00

The number of undergraduates funded by your agreement who graduated during this period and intend to work for the Department of Defense 0.00

The number of undergraduates funded by your agreement who graduated during this period and will receive scholarships or fellowships for further studies in science, mathematics, engineering or technology fields:...... 0.00

Names of Personnel receiving masters degrees

NAME
Total Number:

Names of personnel receiving PHDs

NAME
Total Number:

Names of other research staff

NAME	PERCENT_SUPPORTED
Jason Dahl	0.53
Tia Sharpe	0.14
Sue Martin	0.04
Norm Williams	0.02
Cooper McCann	0.05
FTE Equivalent:	**0.78**
Total Number:	**5**

Sub Contractors (DD882)

Inventions (DD882)

Scientific Progress

See Attachment

Technology Transfer

Scientific Progress and Accomplishments

Foreword

This project entitled "Photon Limited High Resolution Laser Ranging" was an effort funded under the DARPA\DSO Information in a Photon (InPho) program. The focus of the project was to investigate information efficient 1D laser ranging with an emphasis on advanced laser ranging techniques that utilize laser waveforms other the basic brief pulse ranging technique. There were two phases to the project. The first phase lasted from August 2011 through December 2012 and focused mainly the fundamental shot-noise limits of frequency modulated continuous wave laser ranging and demonstrations of the compressive laser ranging technique. During this phase MSU was supported theoretically through a collaboration with Dr. Baris Erkmen of JPL. The second phase was reduced and delayed and lasted from May 2013 through April 2014. The second phase extended the investigation to multiple dimensions and explored imaging utilizing Synthetic Aperture Ladar (SAL) techniques and imaging utilizing compressive sensing techniques. The original program director at DARPA was Dr. Neifeld, with the ARO program manager being Dr. Govindan. The current program director at DARPA is Dr. Kumar. This final report covers the entire effort August 2011 through April 2014 in summary form with extended detail on the last nine months of the effort.

Table of Contents

List of Appendices, Illustrations, and Tables

Statement of Problem Studied

This project seeks to solve the problem of optimizing the amount of information obtained per received photon (bits per photon or bpp) in laser ranging and range imaging measurements. The resolution and sensitivity of laser ranging systems are well known and depend on a number of system parameters including system bandwidth, type of detection (coherent or direct detection), optical background and thermal noise. Less work has been performed to evaluate laser ranging and imaging from an information theoretic perspective, and most studies have focused on transmit waveforms consisting of temporally brief pulses. MSU-Spectrum Lab is developing laser ranging systems based on advanced waveforms to optimize systems for varied applications. In particular, this project investigated two separate laser ranging techniques 1) chirped frequency modulated continuous wave (FMCW) coherent ladar [1] and 2) compressive laser ranging based on transmitting and receiving pseudorandom binary digital waveforms and utilizing ideas from compressive sensing [2]. Both methods have an emphasis on allowing high range resolution without the need for high bandwidth optical detectors and electronics that can limit the resolution, sensitivity, and dynamic range of the laser ranging system. In terms of information theory and efficiency the differences between these methods and simple brief pulse ranging include: 1) the shot-noise limits of coherent detection and conserving and decoding information during coherent processing including Synthetic Aperture Ladar (SAL) processing, 2) achieving optimal photon information efficiency when the range information is not encoded in photon arrival times but rather in the relative power of different transmitted waveforms. In addition to investigating these laser ranging methods, the Phase I effort also included some work on the use of entangled photons generated by spontaneous parametric down-conversion of a chirped source to perform ranging measurements.

Summary of the Most Important Results

Making a post-project self-assessment the scientific results can be categorized into three areas:
1) A thorough experimental and theoretical investigation of the sensitivity limits and information theory of coherent FMCW ladar including the strong LO shot-noise limited regime, the weak LO regime utilizing single photon counting detectors, and extension to multiple dimensions through SAL. 2) Investigations and demonstrations of compressive laser ranging and imaging techniques including compressive 1D laser ranging and 2D imaging at 1550nm with low light levels utilizing Geiger Mode InGaAs APD detectors. 3) Theoretical and experimental investigations toward quantum entanglement of modulated biphotons to enable, demonstrate, and understand the applicability of advanced laser ranging waveforms in the fully quantum regime.

The most significant results of the project were in the first area producing three journal articles, a few conference presentations, and showing significant applicability in MSU's other work in coherent FMCW ladar and SAL imaging. The second area is interesting, but so-far has been less fruitful in demonstrating photon information efficient results, however this area will be pursued further under State of Montana research funding. The third area was eliminated in the second phase of funding due to budget reduction and so at this time remains incomplete. Rather than organizing according to the objectives and tasks laid out in the proposal SOW, this summary will be organized according to these three areas. The summary contains the most important results from each area and provides further details on work occurring after the last interim progress report in August 2013.

Area 1) Sensitivity and photon information in coherent FMCW ladar
FMCW ladar covers many forms of laser ranging which utilize frequency modulated transmit waveforms rather than intensity modulated waveforms. While direct-detect intensity modulated laser ranging systems generally utilize brief pulses and measure the range directly through the delay of the peak return pulse intensity, FMCW ladar system are generally based on linear frequency chirped waveforms, coherent detection of the return pulse against a local copy of the transmit waveform as an LO, and measurement of the range based on the frequency modulation imparted on the detected signal as a function of delay (see Figure 1). The RF spectrum of the heterodyne signal then represents the range profile of the scene. During this project we have used linear chirped FMCW ladar exclusively owing to the advantages afforded by the stretched processing, which allows reduced detector and digitizer bandwidth while maintaining the resolution advantages afforded by our actively linearized chirp laser technology [1].
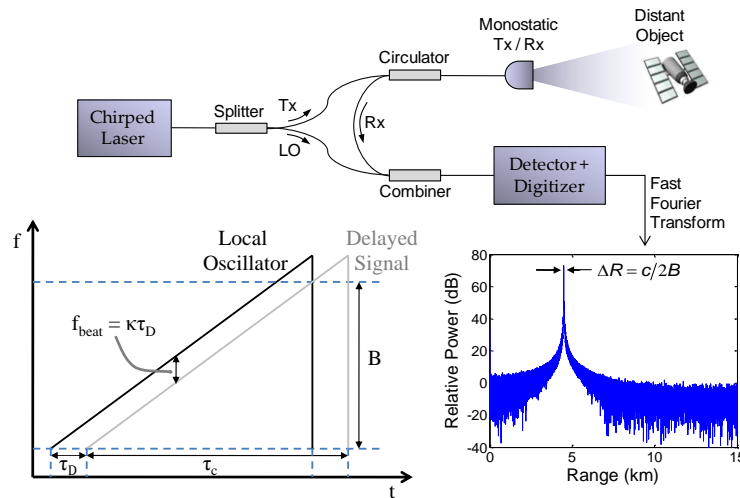
Figure 1 Basic cartoon description of FMCW ladar. The range delay is encoded in the RF spectrum of the detected signal.

1.1 Strong LO FMCW ranging.

Under this subarea we have performed an extensive theoretical and experimental study of the FMCW chirped ladar utilizing balanced heterodyne detection in the strong LO (LO power >> signal power) regime. When the LO power incident on a standard power law photodiode is large enough such that the shot noise of the LO is the dominant noise of the detection system, the detection is said to be shot-noise limited and the sensitivity to photons in the spatial mode of the LO is said to be at the single photon level. Sometimes this is referred to the "shot-noise rule-of-one". A detailed application of the rule shows that for FMCW ladar, where the signal is best observed in the frequency domain, it refers to the carrier-to-noise ratio (CNR). Further we verified the expected non-central χ^2 (Rician) signal statistics which when expressed in units normalized to the shot noise background is:

$$p(z)dz = \exp\left[-(z+x)\right]I_0\left(2\sqrt{zx}\right)dz. \qquad (1)$$

where z is the measured power, x is the mean expected power, and I_0 is the zero order Bessel function of the second kind (see Figure 2).
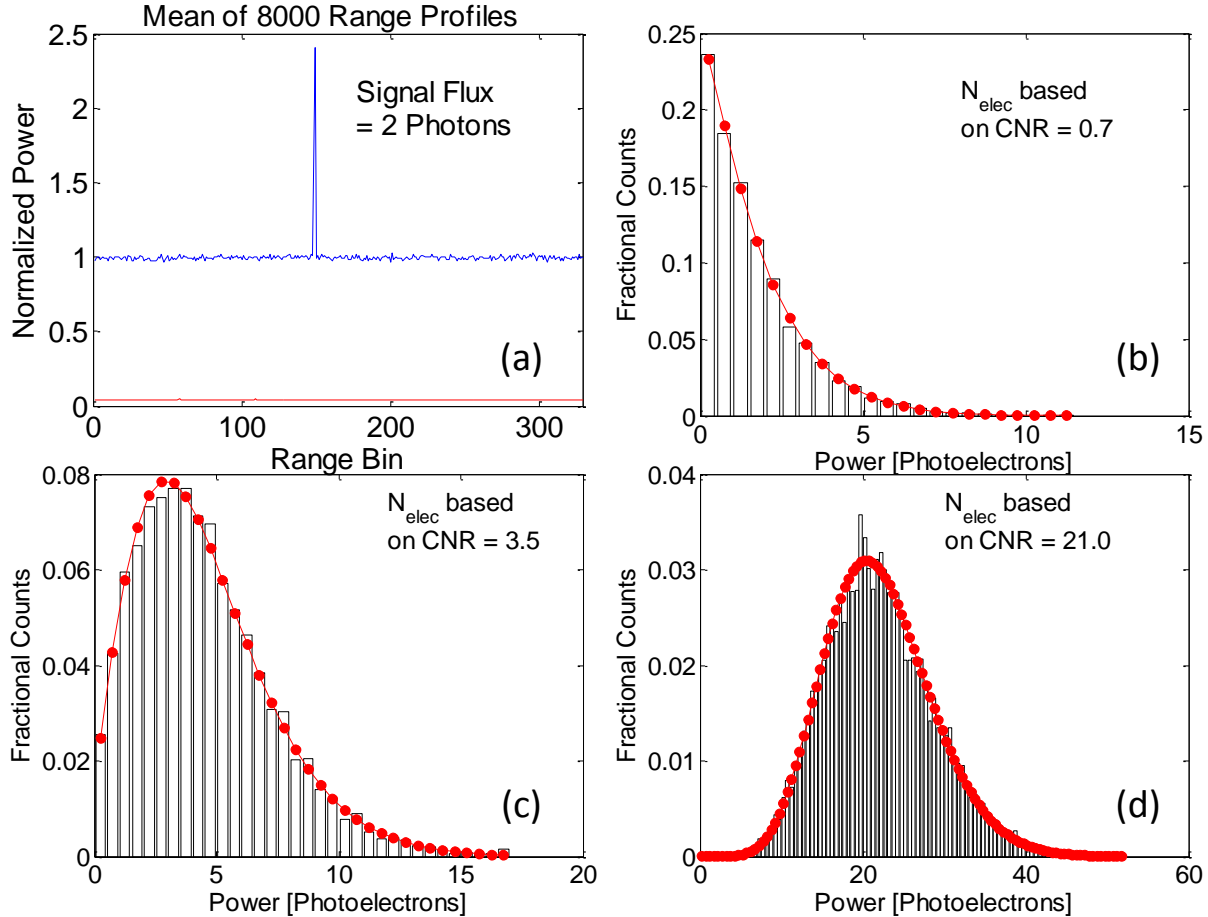
Figure 2 (a) Average of 8000 FMCW range profiles for a signal photon flux of 2 photons per integration period normalized to the background level. The normalized power of 2.4 indicates an average of 1.4 measured photoelectrons. The red line at the bottom is the dark noise of the balanced detector. (b)-(d) Example histograms of the normalized power measured in the target bin for nominal signal flux of 1, 5, and 30 photons respectively. The measured photoelectron flux is consistently 70% of the nominal photon flux. The dotted lines are the corresponding analytic probability density functions.

Moving beyond the simple signal statistics of a single resolvable frequency (range), we investigated the joint statistics of an arbitrary number of resolvable range bins one of which contains the signal from a single delta function range return. This is the statistics involved in the task of locating the position of single specular target using FMCW ladar. The investigation of these statistics led to theoretical calculations of the expected probability of correctly locating the target and the commensurate photon information efficiency (PIE) this task represents. In the end it was determined that the PIE for this task increases toward a maximum of $\log_2(e) \approx 1.44$ bits per photon as a function of the number of resolvable range bins however it approaches this limit very slowly. Additionally, it was determined that the photon flux that produces the peak PIE for a given number of range bins is roughly proportional to the logarithm of the number of range bins. These calculations were verified by experimental measurements.
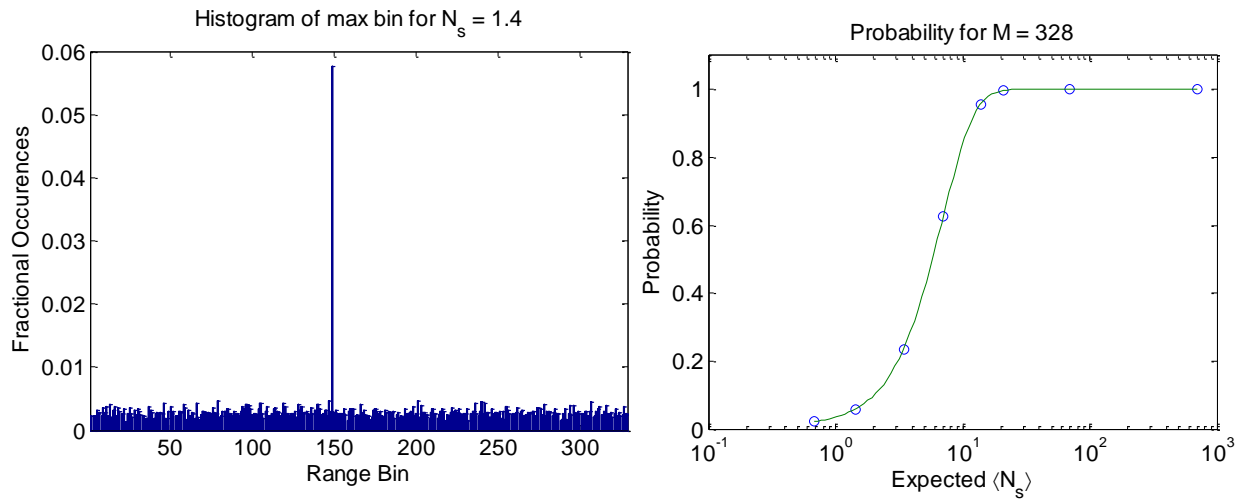
Figure 3 (a) Histogram of 8000 trials of maximum power estimator for target location with average of 1.4 signal photoelectrons per measurement and 328 range bins. (b) The probability that estimator correctly finds the target location for 328 range bins as a function of the mean signal photoelectron level. The open circles are experimental values calculated from the 8000 trials for each of several signal levels.
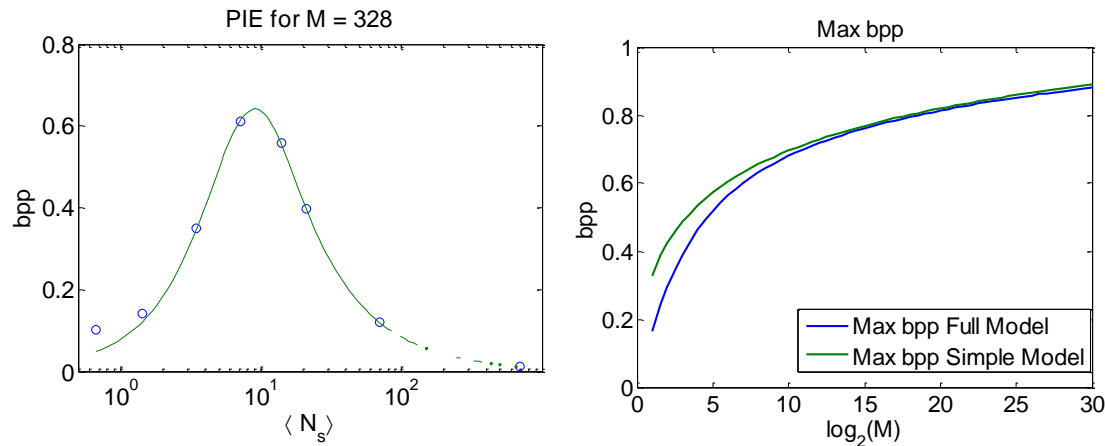
Figure 4 (a) Theoretical and experimental Photon Information Efficieny (PIE) as a function of mean signal photoelectron level measured in bit per photon (bpp) for M=328 discrete range bins. (b) Maximum PIE for task of single target FMCW range location as a function of number of discrete range bins. The PIE approaches a maximum of 1.44 bpp very slowly, making bpp greater than one impractical.

Finally, we investigated other 1D FMCW ladar tasks such as locating two target and/or measuring target amplitudes and determined that these add minimal information to the task. This work was prepared as a journal article and further details can be found in that publication [3].

1.2 Weak LO FMCW ranging

The work performed under this subarea was to investigate theoretically and experimentally the sensitivity and optimal processing of FMCW ladar when the both the LO and signal are low enough to require photon counting detectors. In particular, the use of single photon counting detectors in the form of Geiger Mode APD's provide extra difficulties in the inability to distinguish between single and multiple photon counts, inherent dead-time due to recovery from the avalanche and a need to prevent after pulsing. Dr. Baris Erkmen of JPL the theoretical collaborator for the project provided significant theoretical analysis deriving the Cramer-Rao lower bound for FMCW ranging with coherent laser sources and developing a Maximum Likelihood (ML) estimator that achieves this bound in the photon counting regime.
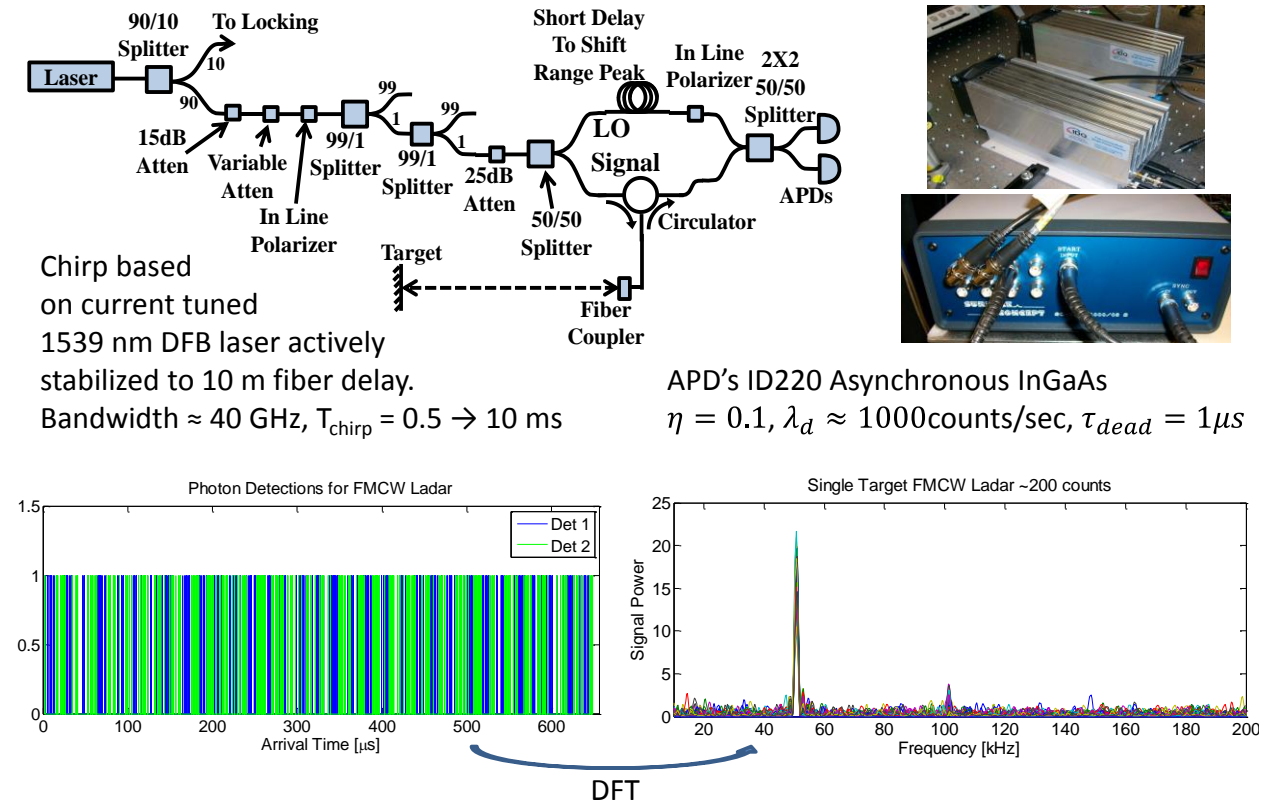
Figure 5 This figure shows the basic experimental setup and results for the weak LO work. The FMCW system had to be designed to produce a reliably small levels of signal flux in both the LO and Signal paths. ID Quantique ID220 Asynchronous Geiger Mode InGaAs APD's were purchased as capital equipment for this and the quantum entanglement portions of the project.

The main result of the theoretical study was to determine a complete analytic description of the Cramer-Rao Bound (CRB) on the uncertainty in range measurements that includes non-idealities of the detectors such as dark counts and dead-time. It was determined that that there are three regimes of the FMCW detection process as a function of the photon flux. At low flux the dark

counts are dominant and the CRB decreases linearly with photon count rate, then at medium photon count rates the noise is dominated by shot noise and the CRB decreases as the square root of the count rate, as the count rate increase the detection becomes limited by the saturation effects of the detector dead-time and the CRB approaches a constant. This result was shown by the analytic model and verified in simulations and experimental measurements (see Figure 6).
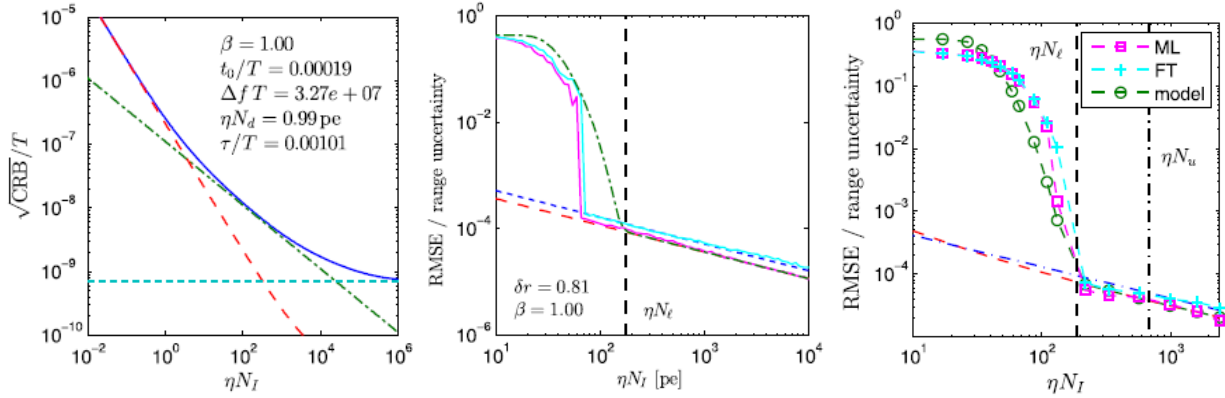
Figure 6 (Left) This plot shows the analytic CRB for the parameters shown in the inset. The different lines show the CRB limits due to dark counts, shot noise, and dead-time. (Middle) This plot shows a simulation of the range uncertainty achieved by the ML estimator. (Right) Comparison of the experimental results achieved by the ML estimator and Fourier Transform (FT) estimator. The ML estimator can achieve 1.5 dB better range uncertainty than the FT estimator in the shot-noise limited regime.

The details of this work are published in an Applied Optics paper [4]. In addition to the scientific results, the expertise gained by MSU in coherent ladar utilizing single photon detectors helped in the progress of a DARPA/STO coherent ladar project that Dr. Barber was involved in with local company Bridger Photonics and Ball Aerospace.

1.3 Sensitivity in Synthetic Aperture Ladar
This area was an extension the work in 1.1 Strong LO FMCW ladar. One of the benefits of coherent FMCW ladar is that measured range profile is phase sensitive, which means that one has access to the detected optical field, rather than just the optical intensity. This measurement of the field allows one to coherently combine the field information from different points in space forming a synthetic aperture which allows one to obtain azimuth information in addition to the range [5]. In the standard form of this process the real aperture of the ladar system is translated in a single dimension and the final image displays one dimension of range (longitudinal) and one dimension in cross-range (transverse). This Synthetic Aperture Ladar (SAL) imaging can be described as sampling the time resolved scattered field from the scene at an aperture consisting of a line perpendicular to the transmit direction, then implementing a computation based lens (i.e. a Fourier transform) to transform this time resolved field to the image plane. When implemented with linear frequency chirped FMCW ladar the 2D image is formed basically by a two dimensional Fourier transform (dimensions of time and aperture position). Being a straight forward extension, the sensitivity and information efficiency aspects of SAL were expected to be very similar to 1D FMCW ranging. While this was largely the result, important aspects that

were studied included: addition of unavoidable speckle statistics of the coherent imaging process, studying the ability to coherently add optical energy where the average return per range profile measurement was below a single photon, and the ability to use information in the image to compensate uncontrollable phase errors due to the imperfect motion of the stage used to implement the aperture motion, particularly when the shot-noise limited SNR was very low.

We have recently submitted detailed results of this work to Applied Optics. The main results are that SAL imaging, including image based phase error compensation can be achieved at very low return levels, including when the average pixel brightness in the final image is near the single photon level. As much of these results have not been reported a copy of the submitted paper is attached as an appendix to this report.
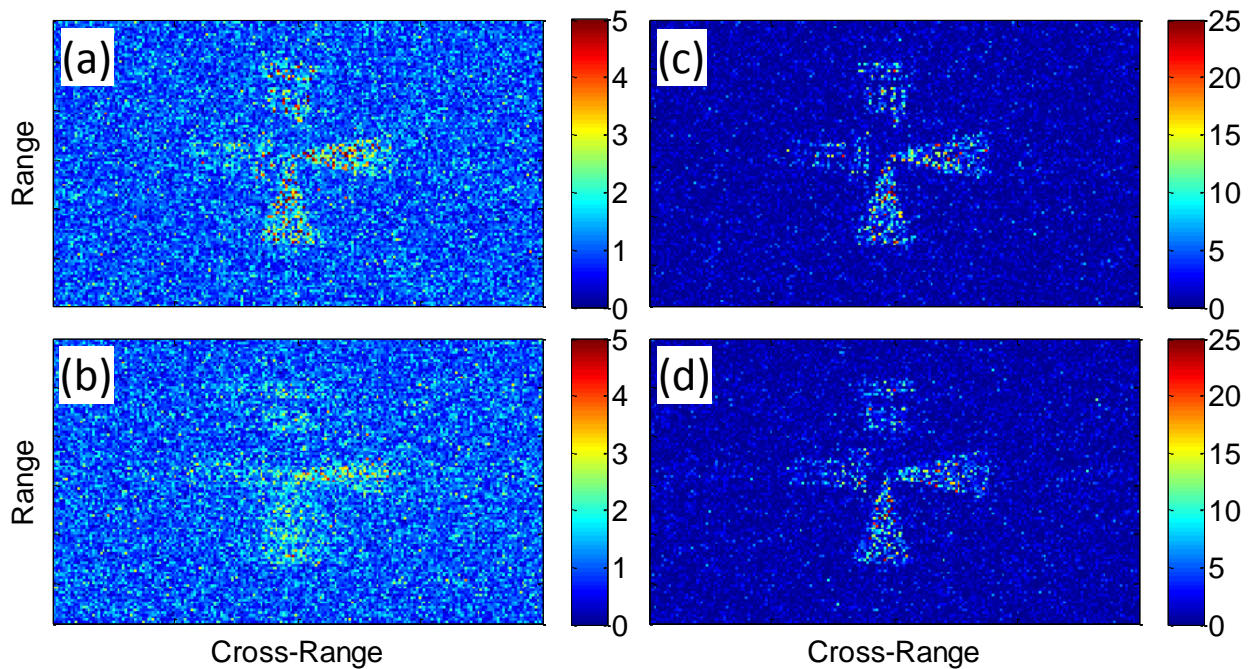
Figure 7 (a) The average of 5 independent 116x200 pixel SAL images with a mean of 1.1 photons per "on" pixel using a bright retro-reflector for phase correction or (b) PGA image (no retro) based phase error correction are shown. The color bars are normalized to the shot-noise background. (c,d) These SAL images are about 5 times higher transmit power and demonstrate marked improvement in the PGA corrected images. No averaging was applied to provide direct comparison with (a, b) at the same total image energy.

Area 2) Compressive Laser Ranging and Imaging

2.1 Compressive Laser Ranging (CLR) Demonstrations

Prior to this project, MSU Spectrum Lab had started the investigation of a new laser ranging technique based on ideas form compressive sensing (CS) and Feature Specific Imaging (FSI) both areas that place an emphasis on using prior information (sparsity in the case of CS and known common features based on training sets or other knowledge in the case of FSI) to choose a measurement basis that allows either reduced number of measurements or improved image formation performance. The difficulty in apply these ideas and techniques to time-of-flight laser ranging was that rather than an inner product measurement like in optical CS or FSI imaging, laser ranging inherently involves a convolution measurement in that the return signal from the

target is the convolution of the transmit waveform with the range profile. To solve this problem, we invented a scheme [2] whereby a modulation waveform is applied both to the transmitted laser and the received signal from the target followed temporal integration then analog-to-digital conversion. The trick of this scheme is that this *multiply by m1 → convolve with SOI → multiply by m2 → integrate* process is equivalent to a *correlate m1 with m2 → multiply with SOI → integrate* process which is just and inner product of the SOI with the waveform formed by the correlation of the two modulation waveforms (vectors) *m1* and *m2*. Once cast as an inner product measurement the theoretical tools of compressive sensing and FSI can be brought to bear on the laser ranging problem. Applying the concepts and results of the experiences with CS based 2D imaging [6], we proposed using pseudorandom binary digital waveforms for transmit and receive waveforms that are created and modulated onto the light using standard telecom techniques. The prior demonstrations were hampered by uncontrollable coherent interference which caused phase sensitive fluctuations of the return signal and prevented the scheme from being used on multiple simultaneous targets.
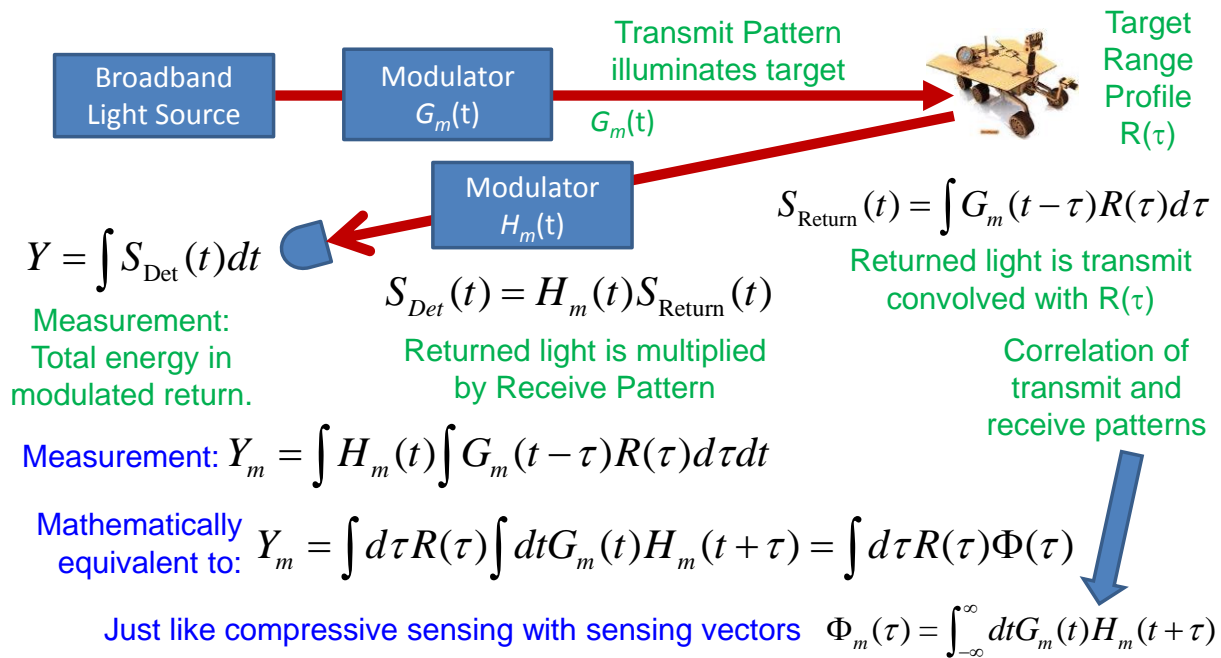
Figure 8 Flow diagram and math showing how the compressive laser ranging (CLR) measurement scheme translates laser ranging into an inner product measurement.

The first task performed in this area on this project was to demonstrate the CLR technique for multiple simultaneous targets. The technique that allowed us to get rid of the coherent interference was to use a low temporal coherence laser source, namely a Super Luminescent Diode (SLD) which has low coherence but high brightness. The CLR demonstrator was very similar to the previous experiments with a few slight changes, and the SLD was sufficient to allow us to detect multiple simultaneous targets consisting of partially reflecting mirrors. The binary waveforms for this demonstration were 128-bits long with 30 measurements were used to detect three targets. The measurements for all six targets were processed with a CoSAMP [7]

algorithms that yielded the locations and amplitudes for the targets. Figure 9 is a plot of the range profile for the mirrors and PRM using the CoSAMP algorithm.
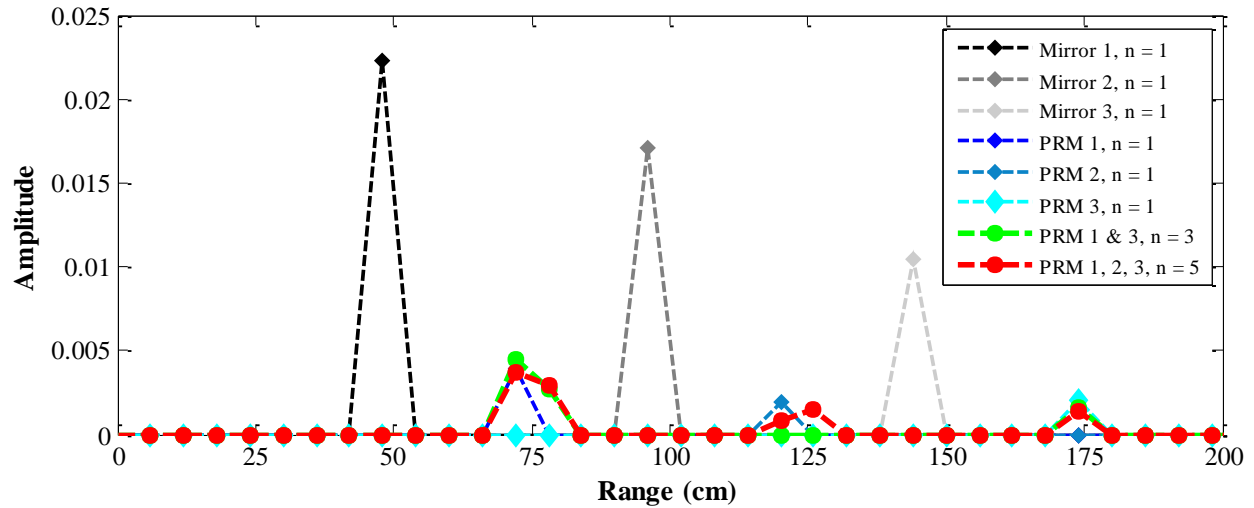
Figure 9 The range profiles for six target positions determined using the CoSAMP algorithm. A) Shows the whole range profile. B) Zoomed in on the range peaks. The black/grey profiles are for the mirrors set at 48 cm, 96 cm, and 144 cm. The blue, red, and green profiles are for the partially reflecting mirrors (PRM) set at 72 cm, 120 cm, and 168 cm.
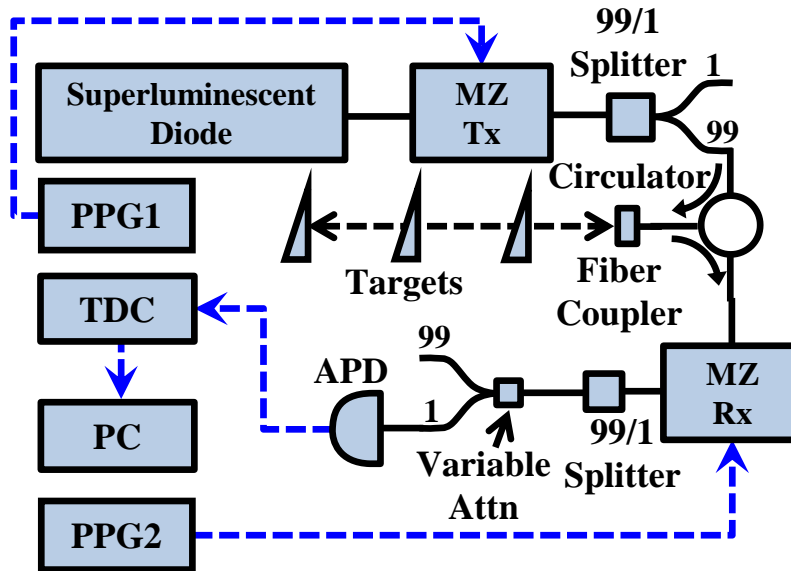
Figure 10 Block diagram of the CLR setup using an single photon counting APD as a detector. Light from superluminescent diode passes into the transmit Mach Zehnder (MZ) EOM. The light is split into one path for monitoring power and the other goes to a circulator and out the targets. After the targets the light passes through the receive MZ EOM and onto the APD. Two 12 Gb/s PPGs were used to replace the AWG that drove the EOMs in the previous demonstrations.

The next task was to demonstrate the CLR scheme utilizing the Geiger Mode single photon counting InGaAs APD's as the detectors instead of linear diodes which require relatively high optical power. The switch to single photon detection proved more difficult than expected due to the need to balance the power hitting the APD's to ensure that it was in the dynamic range

between where the dark counts dominate and the dead-time does not saturate measurements. With these difficulties, we were able to demonstrate the CLR process using the APD's which had the added benefit of allowing us to utilize very fast 10 Gb/s modulation from pulse pattern generators resulting in range resolutions on the couple centimeter level. Despite using the single photon counting detectors large numbers of counts ~60000 per range profile had to be collected to reliably find two targets. This means the practical experimental PIE achieved was extremely small. These results were reported in detail in an SPIE Proceedings article, which is attached as an appendix.
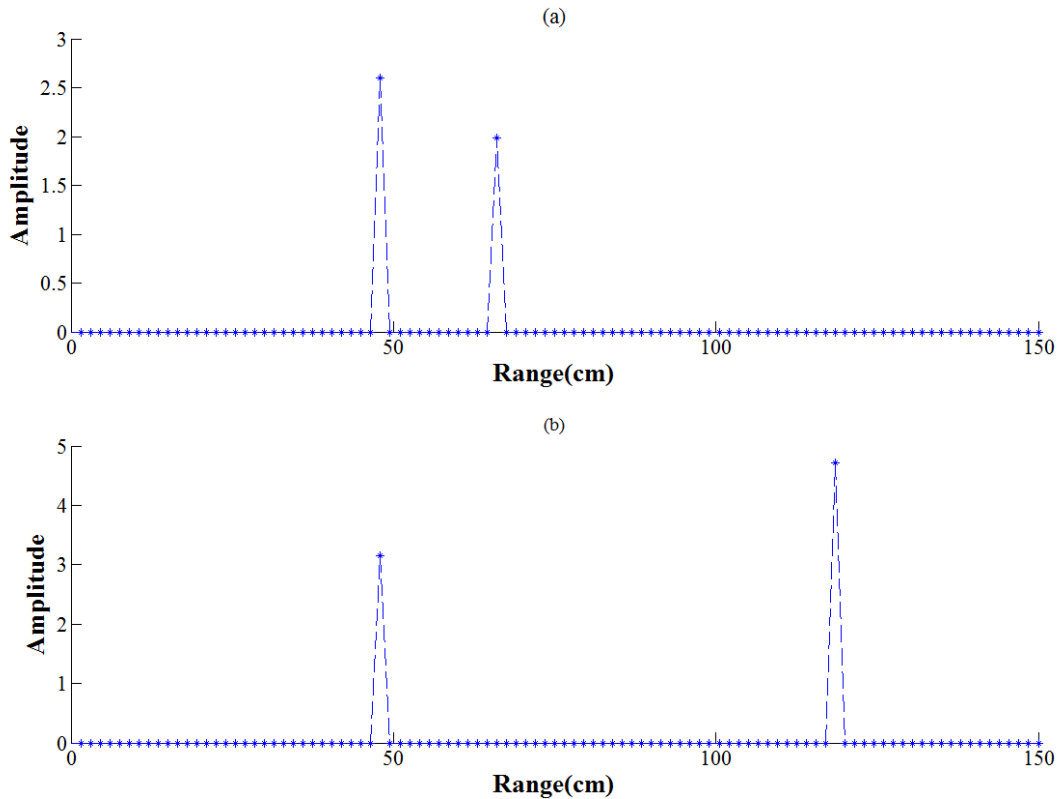
Figure 11 CLR range profile for 1.5 cm resolution setup. (a) Second target 20 cm from the reference target (b) Second target ~60 cm from the reference target.

Due to the poor PIE in the past few months we began to investigate how to utilize the basic CLR scheme to achieve improvements to standard brief pulse ranging. In particular, could one utilize the higher temporal resolution afforded by electro-optic modulators to improve range resolution without losing the PIE achievable utilizing brief pulse ranging and Geiger mode detectors. For example, the resolution for compressive laser ranging depends on the bit width of the patterns being used. At times the target lies between two bins, which makes it difficult to identify the target or in case of two targets closer than the width of a bit to resolve them. The idea of the experiment done here was to try to resolve the ambiguity of the bin location of a target with high efficiency. Waveforms 128 bits in length of alternating 1's and 0's were sent to a target and the return light was modulated with a single pulse per waveform. The waveforms were created using two PPGs and the light was modulated using two EO modulators. The 128 bit alternating

waveforms themselves were sent in an alternating pattern where every even numbered waveform was a complement of the waveform preceding it while the pulses were just sent at set intervals. The pairing made it so that for a certain stationary target, if the pulse multiplying the first waveform overlapped a 1 then the pulse multiplying the second waveform would overlap a 0. A delay of ~33ns between the second PPG and the first PPG was required for the pulses and the patterns to overlap.
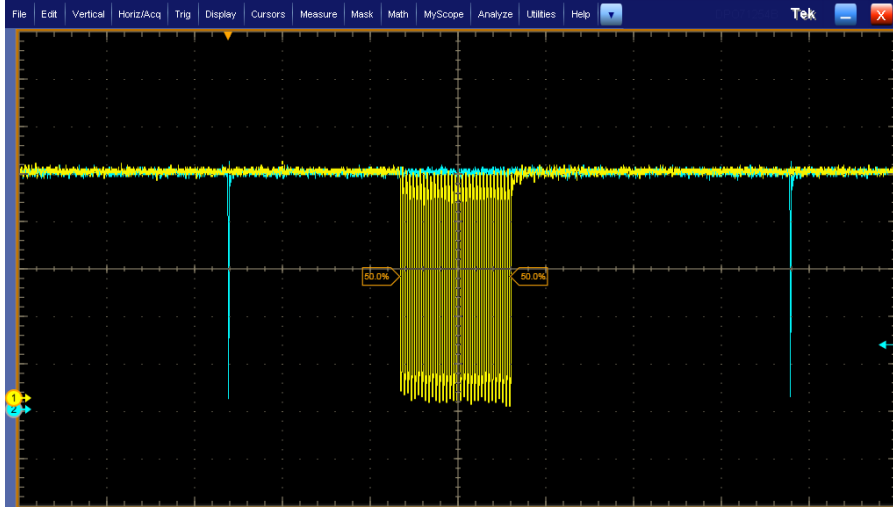
Figure 12 1/0 pattern with a pulse with 33ns delay

The data was collected using the APDs through the TDC and processed using MATLAB. The timing jitter for the APDs is approximately 220 ps and the bin resolution was 80 ps. MATLAB was used to make a histogram plot with a list of times for photon arrivals given by the TDC. This histogram plot is the photon count data for the waveforms and is shown below.
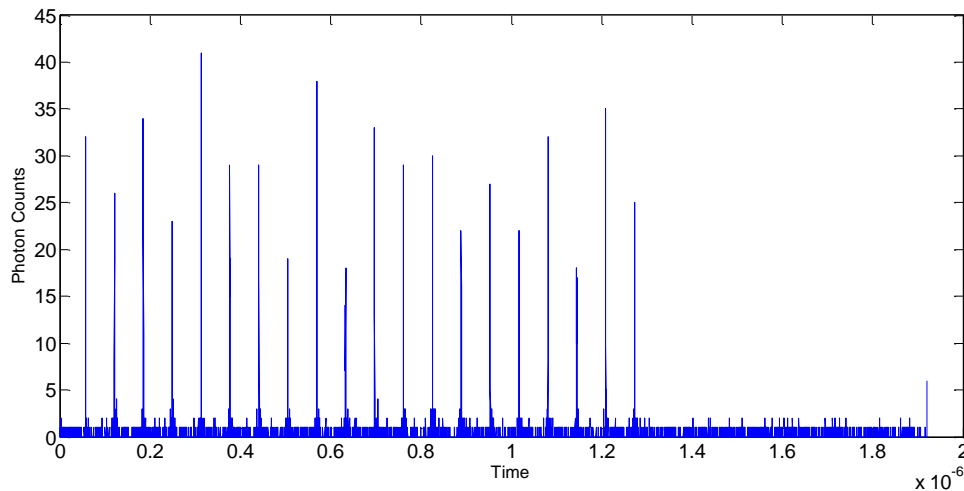
Figure 13 Collected photon counts. Odd pulses are combination of positive pattern and a pulse and the even pulses are a combination of complementary patterns and a pulse.

The long period of zeroes after the last pattern is to account for the dead time of the APDs. Each pattern is punctuated by a number of zeroes in between to account for the delays. As the target is

moved it makes the waveforms and the pulses move with respect to each other. Depending on the bin the target is in or if it is in between bins the number of photons in alternate waveforms will fluctuate. As the target moves between bins, alternate waveforms get more or less counts depending on whether the target is on a 0 or a 1 and it will be alternate in nature. By summing up all the alternate counts and moving the target or slowly shifting the delay between the waveforms and pulses an eye diagram can be seen which gives information about the bin location of the target. A plot of photon counts of the two sets of waveforms as the delay between the waveforms and the pulses is changed is given below.
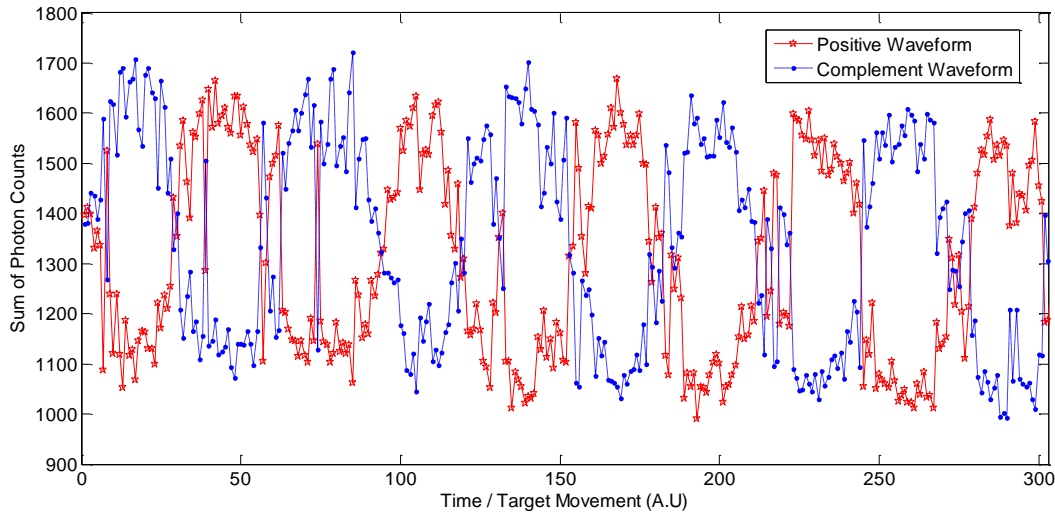
Figure 14 Photon count data of the positive and complementary patterns. Photon counts from all 10 patterns of each set is summed and gives a better contrast.

The intersection point of the red and blue waveforms is where the target is exactly between two range bins. This gives us information about a target location which is more than what is just given by the data rate of the patterns being used. Using this technique it is possible to acquire higher precision of the targets and possibly resolve targets which are closer than the resolution given by the data rate at which patterns are transmitted. This technique is also very photon efficient since less than one photon is being transmitted per pattern. There are 10 patterns in each of the two, positive and complement waveforms. The data set was run for 200ms a piece and there are ~1500 photons per set of data every time a pulse coincides with a 1 on the pattern. An entire waveform is 1.92us long so on average number of photons collected per pattern transmitted is 0.0014. The results are similar to compressive laser ranging where less than a photon is collected for every pattern transmitted. Despite the relatively low contrast shown here, we believe the contrast can be improved and in addition we believe that we can use the "first photon imaging" technique [8] to resolve the rate difference using single or at most two photon counts.

At this point, we would like to mention that the work in this area will continue on a grant funded by the Montana Board of Research and Commercialization Technology (MBRCT). The main focus of this grant is make the linear mode diode version of the CLR system compact by using

FPGA's to produce the pseudo-random binary waveforms, drive the electro-optic modulators, collect the data from an analog-to-digital converter, and then perform the CS processing. As part of the grant, we will also continue to investigate better methods to make the CLR technique photon efficient.

2.2 2D Compressive Imaging at 1550nm

We have finished work on a 2D transverse single pixel camera imager at 1550 nm which utilizes low transmit and return powers, down to the single photon level on the return, and random binary 32 x 32 pixel transmitted waveforms to compressively reconstruct the target image. The 32 x 32 pixel array images are generated using a digital mirror device (DMD) that we can program with up to 960 1 bit images. Figure 15 shows the DMD and an example of one of the transmitted pixel patterns.
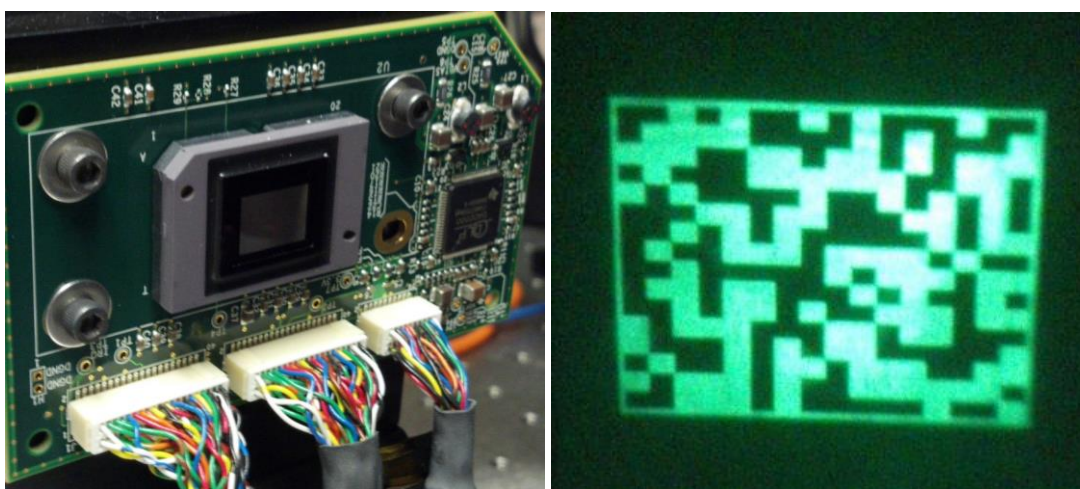
Figure 15 The picture on the left is of the digital mirror device DMD that is used to generate the transmit images. The image on the right shows one of the transmitted images (16 x 16 in this case) seen through an IR imager.

A software interface was created using Matlab that both creates the transmit waveforms and can control the functions of the DMD. The interface can be used to flip and rotate the images, change the frequency at which the images are displayed, adjust the trigger in/out, and start or stop the image cycle. The DMD has a total of 1024 x 768 pixels which we group into an array of 16 x 16 or 32 x 32 larger pixels because we do not need the full density for the type of imaging we are trying to perform.

The DMD mirrors rotate at about 12 degrees from the corners so the deflected light comes off at odd angles. In order for the beam to come off the DMD straight it needs to come in at a 12 degree angle up or down from the corner. This makes alignment of the device a little more challenging. Due to the small size of each pixel on the DMD there is also a lot of diffraction scattering, the device acts like a grating, off the device which reduces the transmissions due to the scattered light and causes further difficulties with alignment.

Figure 16 show a diagram of the optical setup for this project. There are two different laser sources used; the initial source is a 794.5nm distributed feedback laser (DFB) that was used for most of the setup and validation of the imaging system because this wavelength is easier to see which facilitates easier alignment. The main experimental laser is a 1550nm super-luminescent

diode (SLD) as the wavelength of the APDs are in the IR. We also plan to use this laser in conjunction with a second compressive laser ranging setup to hopefully create 3D compressive images.

Following the laser is an output coupler and two lenses (25mm and 300mm respectively) used to expand the beam size so that is fills the DMD. Three mirrors follow which are used to align the beam onto the DMD. The center order from the diffraction contains the majority of the energy so we chose to only utilize that in our design. Following the DMD we have some transmit optics that consist of a 300mm lens that focuses the image onto the target and an iris that we use to select out only the center image from the DMD.
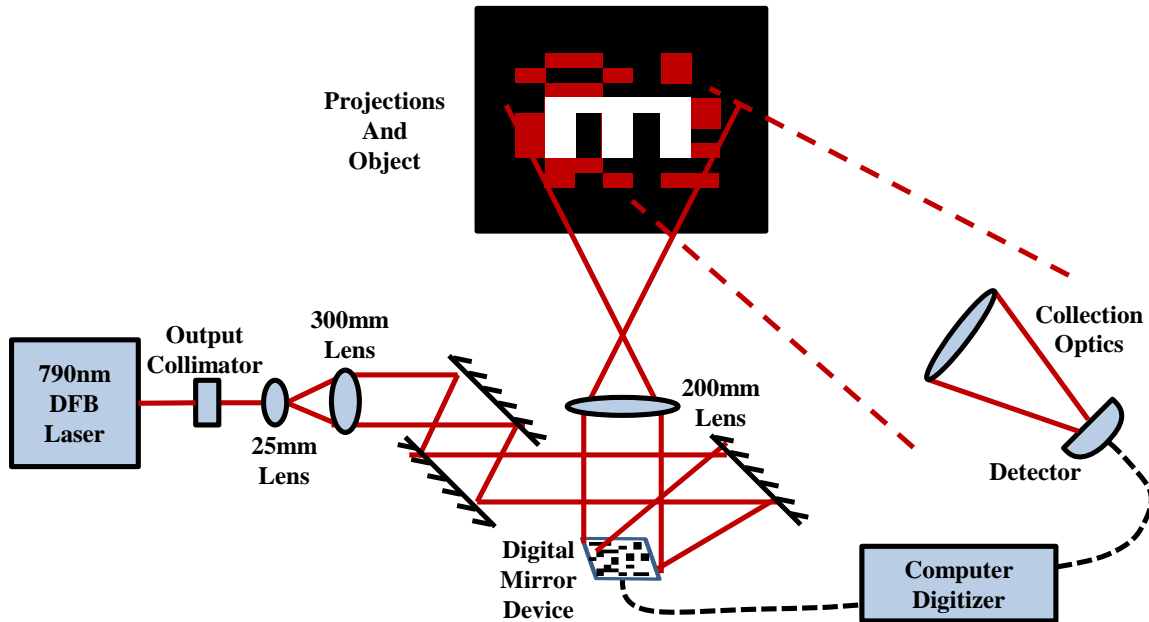
Figure 16 A block diagram showing the components in the optical setup.

The images are projected onto a specular black surface (low scattering to minimize background radiance) to which a target of white card stock, or retro tape, is affixed, Figure 17 is a picture of the actual setup (left) and a picture of the target and background (right). The light scatters off the target and is collected via a 60mm 2" lens and imaged onto a home built 10mm x 10mm (5mm radius for the 1550nm version) 800nm photodetector for the high photon imaging or it is collected using two lenses (14mm and 50mm) into a fiber for the low photon APD version.
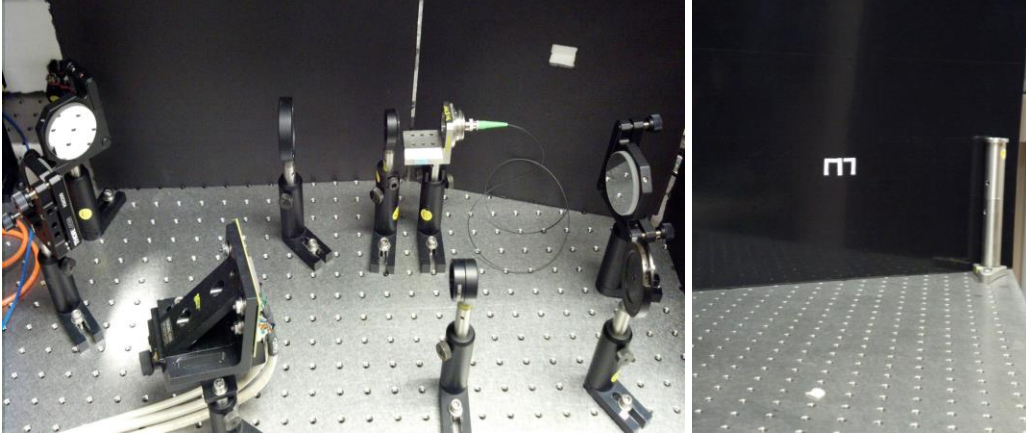
Figure 17 The picture on the left is of the actual optical setup and the picture on the right is of the target and diffuse background.

The backend for the higher power measurements consists of a National Instruments 5122 DAQ (NI5122) and a computer running Matlab. We use Matlab for the post processing which consists of acquiring the data from the detector with the DAQ. The region of interest is cut from the data and the voltage for each frame is averaged over 20 points. We are using an inversed pair of transmitted images so that we can subtract them to remove any background noise. The averaged data is run through a compressive sampling matching pursuit (CoSaMP) algorithm that uses matrix multiplication between the captured data and the known waveforms to recreate the target image.

Figure 18 shows images from two different sets of data at two different distances. The DMD was running at 1kHz with 900 random 32 x 32 pixel frames, 450 after processing to remove background. The averaged data and known transmitted frames are processed in the CoSaMP algorithm along with the number of pixels you want it to search for. For these images there were 74 pixels that made up each image and the algorithm was able to find them all at both the 1.5m and 2.5m distances.
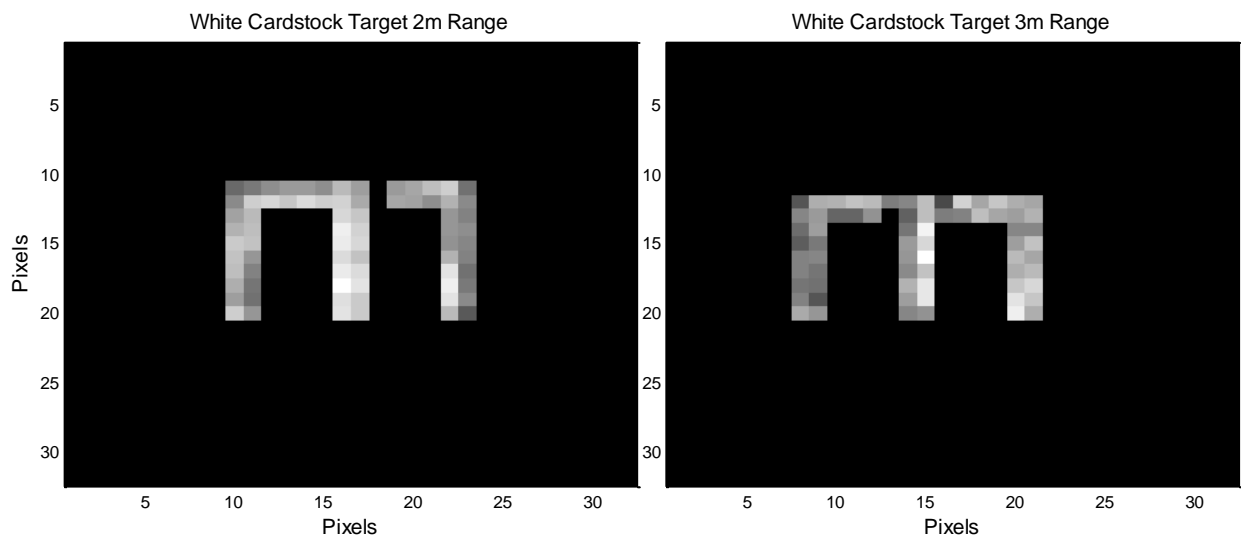
Figure 18 Two different images after processing. The image on the left is at a distance of 1.5m and the image on the right is at a distance of 2.5m one way.

What makes this particularly good is the compressive sampling used to do the images. We have a relatively low bandwidth, 15kHz, single pixel detector that is being used to image at much less resolution then normally would be required to image the same target with low output power 2mW CW to the target, and even less return photons, ~30nW. This process can also be utilized at the single photon level for the return photons and replacing the single pixel detector with an avalanche photo diode (APD).

Low Photon Imaging

After finishing the high power demonstrations we altered the system to start work on low photon imaging. The first change we had to make was with the collection optics. We needed to collect the return into a fiber to be used with our APD. To do this we are using a fiber pigtail that is mounted in a mirror mount. Using a 14mm and 50mm lens, and sending a laser back through the collection optics, the output beam is aligned with the target and the diameter is set to be approximately the same size as the projection waveforms used in the imaging. Moving to this new collection set up means that the input aperture is very small so the return is extremely small. Using the APD to collect the return required modification of the Matlab program to collect the photon counts from the time to digital converter (TDC). This entailed setting up Matlab to talk to the TDC to get the data and then set up the post processing to find the photons for the correct section of the waveforms and run them through the CoSaMP algorithm.
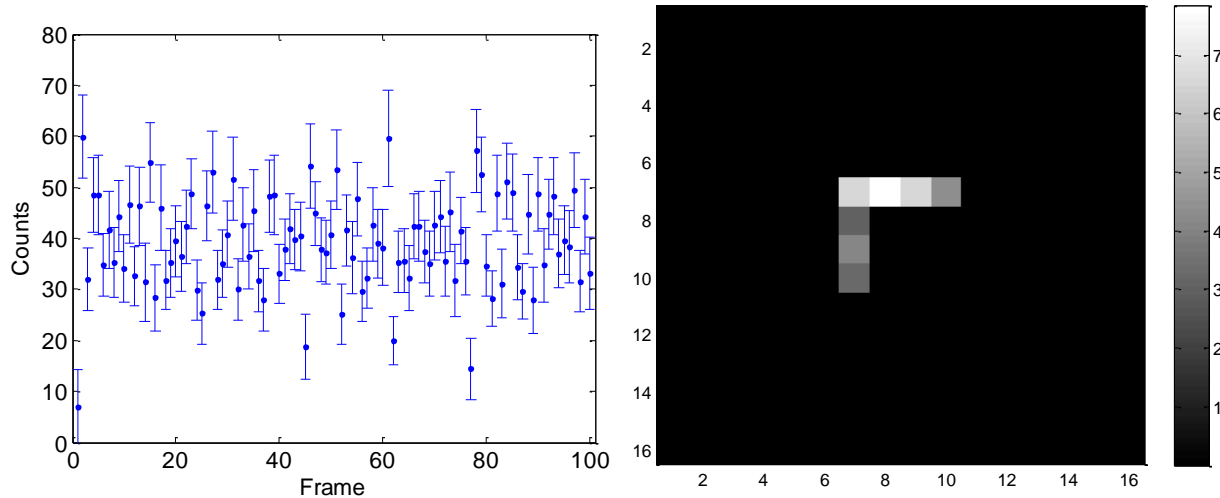
Figure 19 (Left) CS measurements used with CoSaMP to produce the picture at right. Each point represents the mean of 150 measurements for a given frame (projection) in counts. The error bars represent the standard deviation of the measurements. The standard deviation is consistent with Poisson statistics. (Right) Compressive imaging picture resulting from the mean of measurements. The scale is in mean counts from each pixel.

To investigate the photon information efficiency the imaging experiment for the target in Figure 19 left was repeated 150 times. The resulting images were analyzed to determine the number of correct pixels that were found correctly. The number of pixels, k, found correctly translates into a number of bits of information as

$$H_{img} = \log_2 \binom{256}{k}, \qquad (1)$$

which is the logarithm of "nchoosek" or the number of ways that k pixels can be chosen out of the total number of pixels 16x16 = 256. The PIE for that image is then just this entropy divided by the number of collected counts. The histogram of found pixels is shown in Figure 20, which generally shows most of the counts are correctly found. In Figure 20 (right) the resulting PIE for each frame is plotted, the mean PIE is 0.0069. Similar results were found for targets consisting of 4 and 5 pixels, rather than the 7 used here.
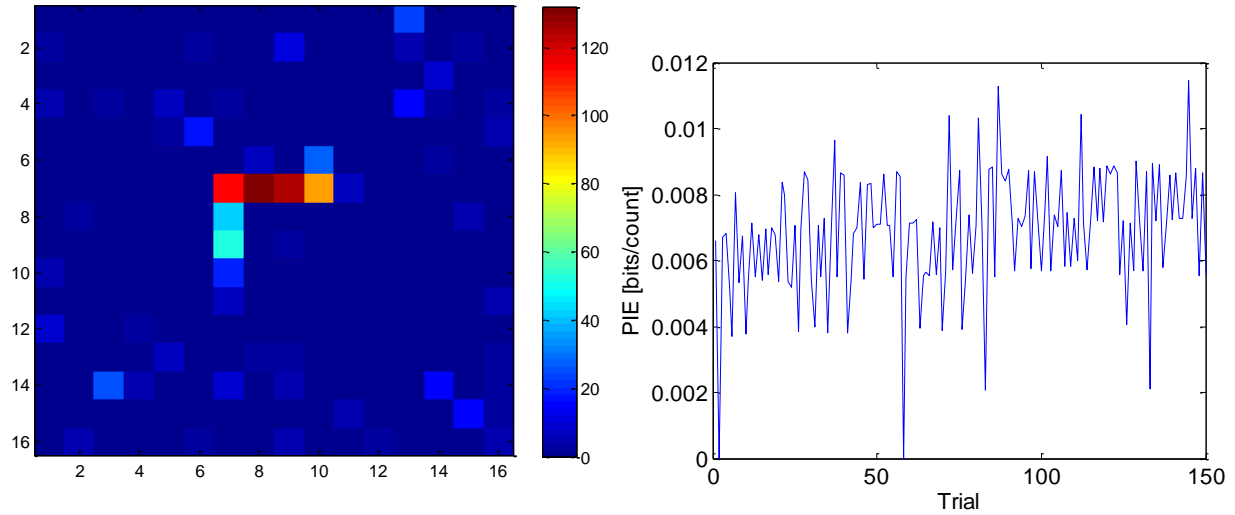
Figure 20 (Left) Histogram of the found pixels. (Right) PIE for each frame, the mean is 0.0069 bits/count.

The use of the "first photon imaging" ideas found in [8] could improve the PIE, however even if sufficient information could be obtained using only a single photon per frame it is unlikely that the PIE would exceed one. This can be determined from a simple argument using standard results in CS. In CS, the number of measurements, M, required to sample a signal with sparsity, S, out of a number of possible elements, N, is generally given as $M > S \log(N)$. However, for purely location information the amount of information scales as the log of nchoosek as in Equation 1 above, which using Stirling's approximation is $NH_2(S/N)$, where H_2 is the binary entropy function. If one photon is used per measurement than the PIE is the ratio, the result is shown in Figure 21. It is interesting that this PIE has a similar shape to the PIE found for FMCW ladar.
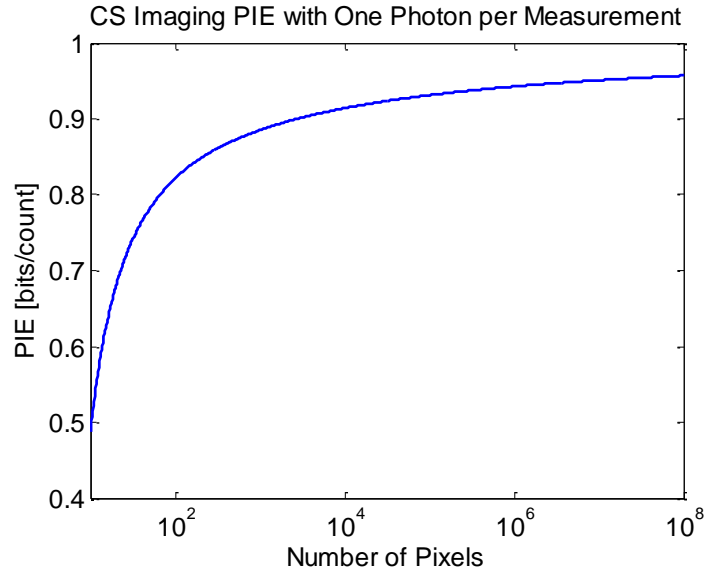
Figure 21Theoretical PIE for CS imaging based on one photon per measurement.

Area 3) Ranging investigations with chirped biphotons

The technical goal of this objective was to demonstrate FMCW ladar with chirped biphotons, but the main scientific inquiry was to investigate how the phase evolution of the pump in spontaneous parametric down conversion (SPDC) is transferred to the signal and idler photons. The purpose being that the strong correlation between the two photons could be used to filter out spurious noise from thermal noise and background counts to increase the efficiency of the photons that are received.

The SPDC device that was used in this project consisted of a Potassium Titanyl Phosphate (KTP) crystal with an ion exchange waveguide to provide confinement and periodically poled for Type II phase matching at a degenerate wavelength of 1586 nm. The device is fiber pigtailed in and out and is packaged with an internal thermal-electric cooler for temperature stabilization. The device was purchased from AdvR Inc., local engineered materials small business. Down-conversion from 793 nm to 1586 nm was chosen to be within the sensitivity region of the InGaAs APD photon counting detectors purchased and to correspond to laser and optics available at Spectrum Lab.

The SPDC device was tested using two main techniques. The first was a Hong-Ou-Mandel (HOM) [10] experiment that showed that the signal and idler beams created degenerate, indistinguishable photon pairs that exhibited a fourth order interference effect when combined with a beamsplitter, see Figure 22 This interference effect only occurs in fourth order (i.e. correlation of photon counts on two detectors), and is generally measured by looking at the coincident count rate between two detectors. The dip corresponds to an effect where two indistinguishable photons that arrive simultaneously at the input ports of a 50/50 beamsplitter will exit out the beamsplitter out the same port together leading to a dip in the coincidence counts on detectors measuring the output of the splitters. This is a quantum mechanical effect, and the contrast we observed is much larger than any possible classical effect.
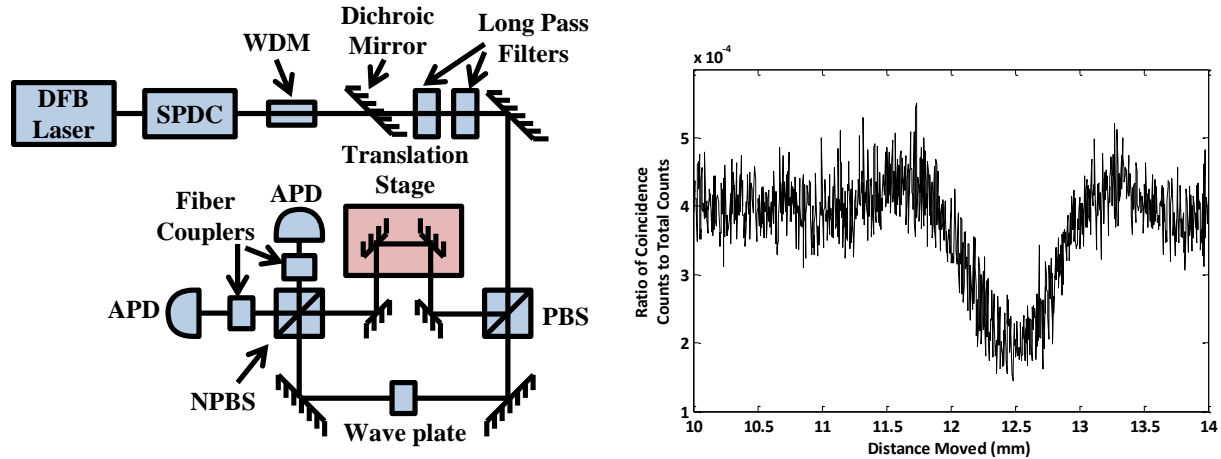
Figure 22 (Left) Diagram showing the setup for the Hong Ou Mandel interferometer. (Left) HOM dips as a function of the translations stage position. Due to the configuration, the relative delay changes twice as much as the position of the stage. For this scan 1001 steps of 4 µm steps over a range of 4mm were taken. The average total counts were 479,690 for 3 seconds with the average coincident counts being 177.

The second technique for testing the quantum properties of the photons from the SPDC source was also similar to the method by which we proposed to demonstrate FMCW ranging utilizing chirped biphotons. This technique is similar to a Franson interferometer that uses a Mach-Zhender geometry [11] (see Figure 23). This type of interferometer is useful to test the mutual coherence properties of the signal and idler photons generated in the SPDC process from the pump. In this experiment one observes fringes in the coincidence counts on the two detectors placed on the output ports of the interferometer. When the delay between the two interferometer paths is larger than the single photon coherence time of the signal and idler outputs second order (i.e. intensity) fringes caused by only the signal (or idler) beams disappear. However, if the signal and idler photons exhibit mutual coherence (i.e. they came from the same pump photon) then the fringes at the sum of the signal and idler frequencies, that is the pump frequency, will be observed in the coincident count rate. The task of demonstrating FMCW ranging with chirped biphotons was to observe these fringes in the time domain for a chirped pump and a fixed interferometer delay, demonstrating that the relative phase of the signal and idler photons would evolve with the sweeping frequency of the pump laser. In the end optical feedback on the pump prevented us from sweeping the frequency of the pump linearly and demonstrating our hypothesis.
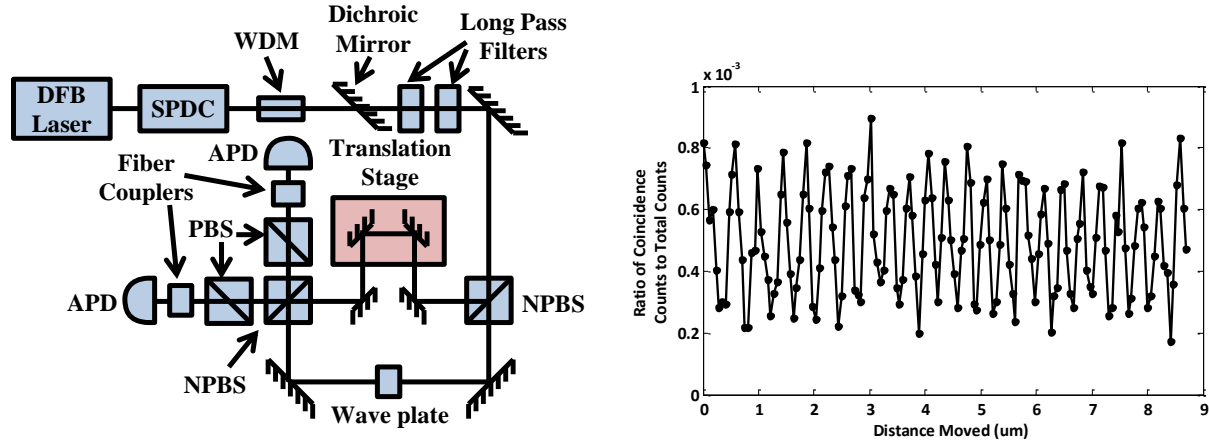
Figure 23 Diagram showing the setup for the Franson interferometer experiment. Shih type two photo interferometer fringes observed in the coincident count in the medium to long delay regime. The fringes show about 75% fringe visibility. The settings for are 151 steps of 58nm each for a range of 8.7um. The average total counts are 109,370 and the average coincident counts are 54.

In the final quarter of 2012, Dr. Erkmen began a theoretical analysis of the properties of chirped biphotons. His investigation is broken into two parts. In the first part, he analyzes the effect of applying chirped modulation to the signal and idler beams after SPDC generation. In this case, he calculated the effect that the application of chirp modulation has on the visibility of the HOM interference, see Figure 24. The upshot is that with the values of chirp rates contemplated 10^{12} to 10^{14} Hz/s^2 that the effect on the HOM interference is negligible. The second part, Dr. Erkmen begins an analysis of the properties of the output of SPDC process for a chirped pump input. In this case he identifies that if the chirp rate is small compared to the phase matching bandwidth (e.g. GHz/s for 10 ps phase matching width) the chirp phase can be ignored and output can be treated as a slowly drifting single frequency pump. However, for the chirp rates contemplated here, ~THz/s, the chirp phase cannot be ignored and a closed form solution with arbitrary phase modulation to the coupled mode differential equations cannot be found. This means that further theoretical investigation will be required.
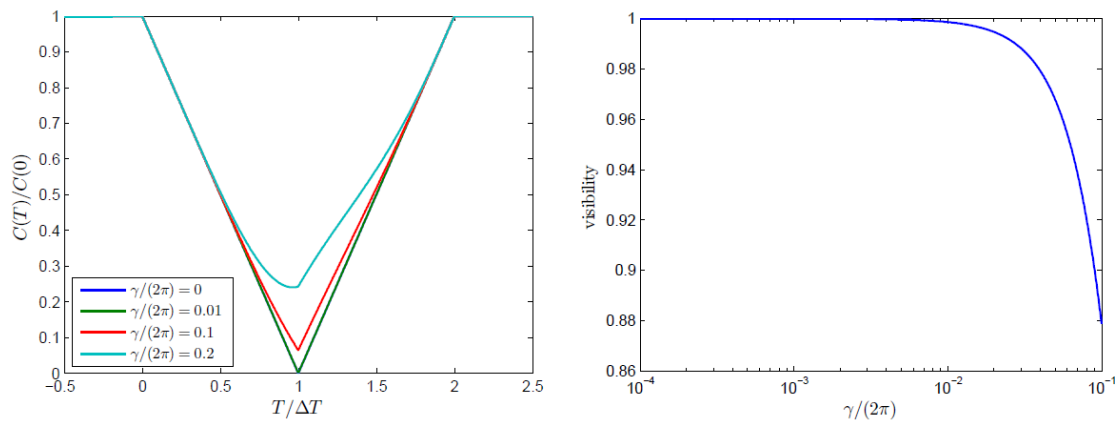
Figure 24 HOM interference with signal and idler biphotons chirped synchronously with identical chirps. (a) The coincidence dip as a function of the relative delay in the interferometer. (b) The visibility as a function of the chirp-induced phase parameter γ.

23

Due to the reduction in the second phase of this project and at the guidance of Dr. Kumar this portion of the project was dropped. At this time there is no plan to pursue further, however we were very close to getting significant results and we might revisit this project as an undergraduate or graduate project.

Bibliography

1. P. A. Roos, R. R. Reibel, B. Kaylor, T. Berg, Z. W. Barber, and W. R. Babbitt, "Ultra-broadband optical chirp linearization for precision metrological applications," Optics Letters **34**, 3692–3694 (2009).
2. W. R. Babbitt, Z. W. Barber, and C. Renner, "Compressive laser ranging," Optics letters **36**, 4794–4796 (2011).
3. Z. W. Barber, J. R. Dahl, T. L. Sharpe, and B. I. Erkmen, "Shot noise statistics and information theory of sensitivity limits in frequency-modulated continuous-wave ladar," J. Opt. Soc. Am. A **30**, 1335–1341 (2013).
4. B. I. Erkmen, Z. W. Barber, and J. Dahl, "Maximum-likelihood estimation for frequency-modulated continuous-wave laser ranging using photon-counting detectors," Appl. Opt. **52**, 2008–2018 (2013).
5. S. Crouch and Z. W. Barber, "Laboratory demonstrations of interferometric and spotlight synthetic aperture ladar techniques," Opt. Express **20**, 24237–24246 (2012).
6. M. F. Duarte, M. A. Davenport, D. Takhar, J. N. Laska, Ting Sun, K. F. Kelly, and R. G. Baraniuk, "Single-Pixel Imaging via Compressive Sampling," IEEE Signal Processing Magazine **25**, 83–91 (2008).
7. D. Needell and J. Tropp, "CoSaMP: Iterative signal recovery from incomplete and inaccurate samples," (n.d.).
8. A. Kirmani, D. Venkatraman, D. Shin, A. Colaço, F. N. C. Wong, J. H. Shapiro, and V. K. Goyal, "First-Photon Imaging," Science 1246775 (2013).
9. J. A. Tropp, J. N. Laska, M. F. Duarte, J. K. Romberg, and R. G. Baraniuk, "Beyond Nyquist: Efficient Sampling of Sparse Bandlimited Signals," IEEE Trans. Inform. Theory **56**, 520–544 (2010).
10. R. Ghosh, C. K. Hong, Z. Y. Ou, and L. Mandel, "Interference of two photons in parametric down conversion," Phys. Rev. A **34**, 3962–3968 (1986).
11. J. H. Shapiro and K.-X. Sun, "Semiclassical versus quantum behavior in fourth-order interference," J. Opt. Soc. Am. B **11**, 1130–1141 (1994).

Appendices

Appendix 1) Article recently submitted to Applied Optics on SAL Imaging.

Synthetic aperture ladar imaging demonstrations and information at very low return levels

Zeb W. Barber[1*], **Jason R. Dahl**[1]

[1]Spectrum Lab, Montana State University,
Bozeman, MT 59717
*Corresponding author: barber@spectrum.montana.edu

We present synthetic aperture ladar (SAL) imaging demonstrations where the return signal level from the target is near the single photon level per resolved pixel. Scenes consisting of both specular point targets and diffuse reflection, fully speckled, targets are studied. Artificial retro-reflector based phase references and/or phase gradient autofocus (PGA) algorithms were utilized for compensation of phase errors during the aperture motion. It was found that SAL images could reliably be formed with both methods even when the final max pixel intensity was at the few photon level which means the SNR before azimuth compression is below unity. Mutual information based comparison of SAL images show that average mutual information is reduced when the PGA is utilized for image based phase compensation. The photon information efficiency of SAL and coherent imaging is discussed.

OCIS codes: 280.3400, 030.5290, 000.5490,280.6730

1. Introduction

Synthetic aperture imaging ladar (SAL, SAIL) has attracted renewed attention as an imaging modality that can complement other electro-optical sensor systems such as synthetic aperture radar (SAR), passive visible and IR imaging, and other active lidar/ladar imagers. In comparison to other optical systems, SAL techniques provide image resolution beyond the diffraction limit of the real optical aperture, the ability to image at night/low light level situations, and require relatively low resources. In comparison to SAR, SAL requires much less relative aperture motion for a given azimuth resolution, can support more signal bandwidth for improved range resolution, and provides better directivity of emissions. In part, the interest in SAL is driven by innovations in broadband coherent ladar sources and systems including chirped frequency modulated continuous wave (FMCW) ladar, coherent pulsed, and digital signal modulation and processing methods that support centimeter to sub-millimeter scale range resolution, which makes the SAL azimuth resolution enhancement techniques more useful [1–3]. Recent SAL work in the literature includes table-top scale laboratory demonstrations [4–6] and demonstrations from an aerial platform [7] .

The two main practical issues with SAL are poor photon budgets resulting from single-mode diffraction limited collection, and the need to correct motion induced phase errors for proper SAL image formation. In earlier SAL work [8], we found that image based phase compensation with phase gradient autofocus (PGA) algorithms did a qualitatively good job of estimating and compensating very large phase errors even with low levels of collected return light. This work extends our information theoretic analysis of FMCW ranging [8] to better quantify the sensitivity and performance of SAL imaging and PGA compensation algorithms at very low return light level.

2. Speckle in Shot-Noise Limited Coherent Heterodyne Measurements

The theoretical and experimental results we presented in [8] described the signal statistics and information theory for one dimensional FMCW ranging for range-resolved, specular targets. The main result of this work was to modify the standard single photon sensitivity rule of coherent heterodyne detection for target range location with a logarithmic scaling of sensitivity based on the number of resolvable range bins. While that analysis should hold for any coherent measurement of well resolved specular targets, including SAL imaging, most real-world situations are not this idealized. In particular, if the targets are not range resolved or, in the general case of SAL imaging, consist of unresolved diffuse scattering targets, the analysis has to be modified to take into account the statistical distribution of the return signal collected into the spatial mode of the LO, namely speckle. The resulting RF signal power (z) for shot-noise limited coherent detection is given by a non-central χ^2 (Rician) distribution, which when normalized to the mean of the LO shot-noise is simply

$$p(z)dz = \exp\left[-(z+x)\right]I_0\left(2\sqrt{zx}\right)dz \qquad (1)$$

Here x is the amount of signal power in the spatial mode of the LO scaled in units of signal photons received in the mode of the LO. (Note: Photons and photoelectrons may be used interchangeably throughout this paper; however the quantum efficiency of the photodiodes can merely be included as an extra optical loss before the detector.) When ranging to a diffuse target as in SAL the signal power in the spatial mode of the LO will vary owing to the coherent addition of the many randomly phased scattering points at the same unresolved range producing a speckle distribution [9]. The mode selectivity of coherent detection prevents any speckle averaging of the collected signal so the speckle distribution is fully developed. This results in an exponential distribution of power in the mode of the LO as $p(x)dx = (1/\lambda)\exp(-x/\lambda)dx$, where λ is the mean return signal power. Combining this distribution with

Equation 1 and integrating over x produces the distribution of a shot-noise limited coherently detected speckle target,

$$p(z)dz = \frac{1}{1+\lambda}\exp\left[\frac{-z}{1+\lambda}\right]dz \qquad (2)$$

Perhaps unsurprisingly, this is an exponential distribution (like the parent speckle distribution) that also converges to the proper zero signal field coherent heterodyne result.

As in Ref [8], we can use this probability distribution to calculate the sensitivity for target location tasks in ranging and/or SAL imaging, by calculating the probability of correctly locating a single target among a number of unoccupied locations (range bins, or image pixels). This probability is found by averaging the probability that the target produces a measured signal power z and that the unoccupied locations show a measured signal power less than z, over all possible values of z. This probability is given by the integral:

$$P_{cor} = \int_0^\infty \left(1-e^{-z}\right)^{M-1}\frac{1}{1+\lambda}\exp\left[\frac{-z}{1+\lambda}\right]dz \qquad (3)$$

Through a simple $u = e^{-x}$ substitution integral this can be expressed in a standard form found in the CRC integral tables [10], giving a simple closed form solution as

$$P_{cor} = \frac{1}{1+\lambda}\frac{\Gamma\left(\frac{1}{1+\lambda}\right)\Gamma(M)}{\Gamma\left(\frac{1}{1+\lambda}+M\right)} \qquad (4)$$

(a)

Probability of Locating Target in 100 bins
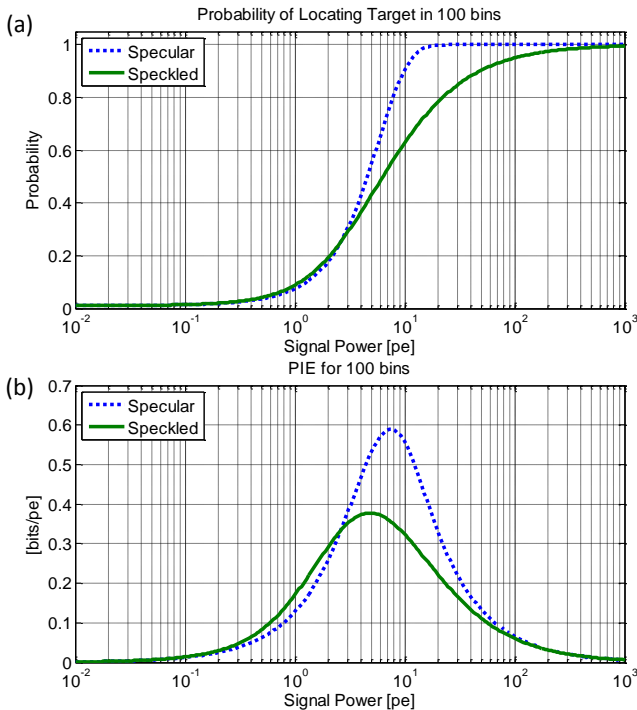
(b)

PIE for 100 bins

Figure 1 (a) The probability of correctly locating a target among 100 resolvable range bins or pixels for shot noise limited coherent heterodyne detection for both specular (dotted line) and speckled (diffuse scattering) targets (solid line). (b) The resulting theoretical photon information efficiency based on (a).

From this probability distribution, we can also calculate the theoretical photon information efficiency (PIE) for this task as shown in [8]. It should be noted that Equation 10 in [8] has a typo and should read

$$H(X|Y) = -P\log_2 P - (1-P)\log_2\left(\frac{1-P}{M-1}\right) \qquad (5)$$

Figure 1 visually compares these expressions for the probability of correctly locating the target and commensurate PIE to the results for a specular target. As one can see the main effect of speckle is to dramatically soften the threshold behavior in the probability of location as a function of mean return power. Additionally, while the PIE is reduced for speckled targets relative to specular targets, the peak photon efficiency is shifted to lower mean return level. Together this suggests that speckle hurts the performance of coherent ranging and imaging but not dramatically at low mean return levels.

3. Experimental Setup

The SAL imaging measurements were performed using a table-top setup consisting of a chirped laser based on a telecom semiconductor DFB laser at 1.54 µm whose chirp is actively stabilized to a 10 m fiber delay. The laser is chirped with a triangle wave fashion and maintains phase lock at the turn around points so that the center frequency of the laser chirp is also stabilized to the fiber delay. The center frequency is occasionally monitored by observing the transmission through an HCN cell and any slow drift is corrected manually. The good absolute frequency stability of the fiber delay line removes the need to reference the start frequency of the data collection to the HCN transmission as in [5].

The entire setup uses fiber based components for amplification, splitting and recombining the LO, transmit, and received optical signals. The free-space portion of the optical setup consists of only a polarization maintaining dual-fiber ferrule that is used to both illuminate and collect the scattered light from the target scene. By illuminating the scene with the bare output of one single mode fiber and collecting the scattered light with the other, the need for an optical circulator is eliminated and the interference from stray reflections in the fiber path is greatly reduced. This is particularly important when using the extremely small real-aperture from a fiber as the path loss can exceed 130 dB for meter distances. The close spacing (250 µm) of and the large divergence (~.11 NA) out of the bare faces of the single mode fibers means that in the far field the modes of the fibers are well overlapped. The received light is mixed with approximately 200 µW of LO power using a 50/50 2x2 fiber splitter and detected with a homemade auto-balanced detector to ensure maximal cancellation of residual intensity noise. A 100 Ms/s 14-bit resolution NI-5122 analog-to-digital converter (ADC) is used to capture the heterodyne signal. Prior non-imaging FMCW ladar experiments verified that this setup is dominated by shot-noise and has a quantum efficiency of ~70%. [8]

Targets were placed 2 meters from the aperture using a black-specular acrylic material as a low scattering dark background. The targets were inclined approximately 60
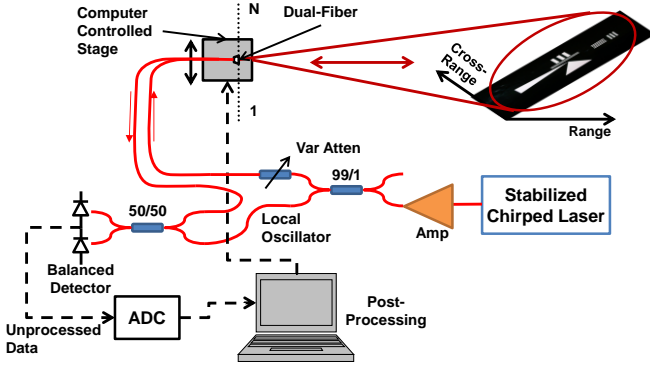
Figure 2 shows a schematic of the experimental setup. All the fiber components are polarization maintaining. The transmit/receive optics consist of a two bare fibers mounted in a single ferrule with a spacing of 250 μm. The amplifier was either a semiconductor optical amplifier that provided up to 80 mW of power, or an EDFA which could provide up to 1 W of power.

degrees away from the transmit/receive (Tx/Rx) optics to provide range diversity. The Tx/Rx optics were mounted on a computer controlled stage to provide motion perpendicular to the transmit direction. The chirp rate of the laser was set to 33.3 GHz/ms at a 200 Hz repetition rate. The total time captured by the ADC was 2.3 ms for each range profile measurement corresponding to a bandwidth of 76.6 GHz or 2 mm range resolution. The aperture motion varied from experiment to experiment, however generally the total aperture size was 0.75 mm giving a cross-range pixel size of approximately 2.1 mm at the 2 meter target range. The transmit power could be adjusted using a variable fiber attenuator.

4. SAL Imaging of Specular Targets

The first target to be studied consisted simply of two cat-eye retro-reflectors separated by about 15 cm in cross-range and 1.6 cm in range. The aperture motion was set to take 500 steps and 138 range bins were stored for 25 runs. The data was processed so that an independent image was formed by taking every fourth step generating 100 independent 125x138 pixel SAL images. This collection was repeated for several different transmit power levels, including levels for which the return level from each reflector was on average less than 1 photon per aperture position. Figure 3 and Figure 4 show the results for a single image taken at a power level such that the average return from each reflector was about 0.5 photons per aperture step.

Figure 3 shows the SAL image before the PGA algorithm is applied, in this image the targets are unobservable due to the cross-range spreading caused by phase errors during the aperture collection. However, the range of the two targets can be identified in the mean range profile shown by the blue trace to the right of image. After the PGA algorithm is applied to estimate and correct the phase errors the targets become observable directly in the image representing nearly complete recovery of the aperture coherence (see Figure 4). The PGA algorithm in this case was modified to search for the 4 range lines with the most power and apply the PGA algorithm using the phase estimation from those ranges only. When PGA was applied to the whole image the phase
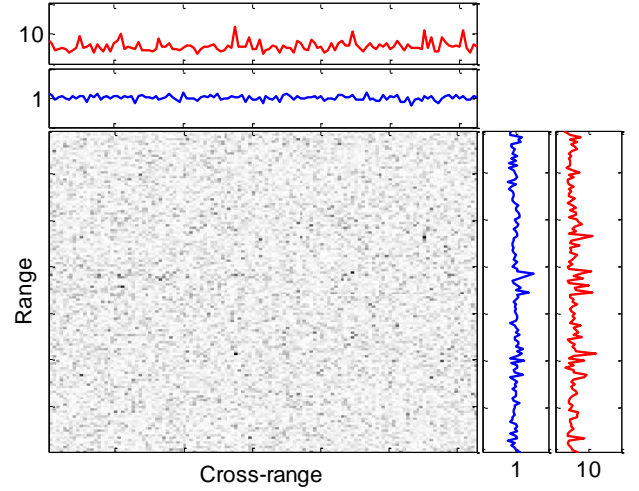
Figure 3 An example SAL image before PGA of two cat-eye retro targets with an image size of 138x125 pixels. The plots on the edges of the image are the mean (blue) and max (red) of the image along range (top) and cross-range (right). The correct ranges of the two targets can be seen in the plot of the mean on the right, but the targets are basically unobservable in the image. The image scale is scaled so that darker is indicates higher intensity. The scales on the plots at top and to the right are scaled such that the shot noise background is normalized and the power reflects the measured return signal level in photoelectron*s*.

more signal power was required to effectively recover the aperture coherence. An additional issue with the PGA algorithm was that the large initial spreading in cross-range led to independent images becoming shifted in cross-range. Finally, Figure 5 shows the result of using 100 independent images to estimate the average amount of information represented by the task of locating two targets in the image. The maximum information represented by locating two targets in an $N \times M$ image is

$$H = \log_2 \left[\binom{NM}{2} \right] \qquad (6)$$
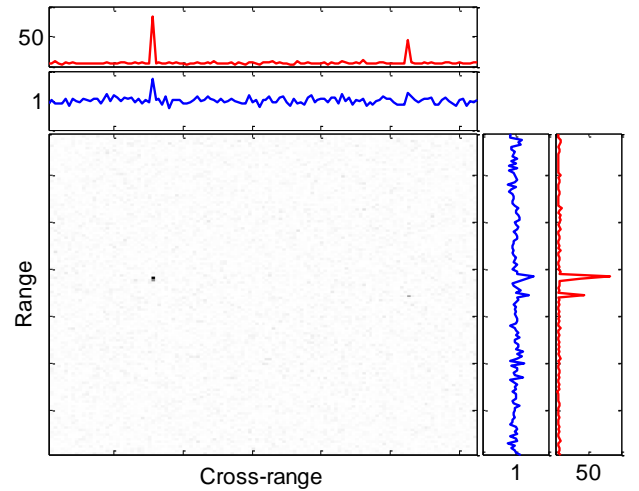
Figure 4 The same SAL image as in Figure 3 after PGA. The correct range and cross-ranges of the two targets are easily observed in both the image and the max plots (top-top and right-right). As one can see in the mean in the cross-range direction (1st plot to right) is identical to that of the pre-PGA image.
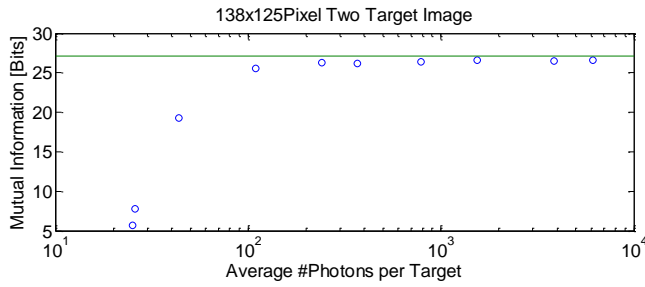
Figure 5 The mutual information of the two target scene estimated from 100 independent images at different power levels.

that is the logarithm of "nchoosek" for the number of targets (2) of out of the total number of pixels $(N * M)$. If one calculates the peak PIE from this data one obtains a value that is significantly smaller than that predicted by the results in [8] (~0.25 vs. ~0.76 bits/pe). This reduction in PIE is likely due to the extra processing required to recover the phase information with the PGA algorithm. If there were no phase errors during the aperture collection than PGA is not required and one would expect to recover close to the full theoretical PIE. Despite this, the results show that for this two target image nearly all the location information can be obtained with only 200 signal photons, which is about 1% of the energy contained in the shot-noise background..

5. SAL Imaging of Diffuse Targets

In order to study the sensitivity and performance of the SAL imaging process under more realistic scenarios, we constructed a relatively complex test target consisting of strips and triangles cutout of bright white card stock that were arranged against a dark background forming a high contrast binary test target (see Figure 6). The heights of the triangles are 9 cm and the bases are 5 cm, the different sets of lines are spaced at 5 mm and 2.5 mm pitch. The total area of the white or "on" portions of the scene is 6500 mm^2 which corresponds to about 1300 "on" pixels in the scene when projected onto the range – cross-range plane. The transmit beam at the target is approximately Gaussian with a beam radius of approximately 20 cm giving an average illumination intensity of 8 µW/mm^2 per mW transmit power. Assuming Lambertian scattering
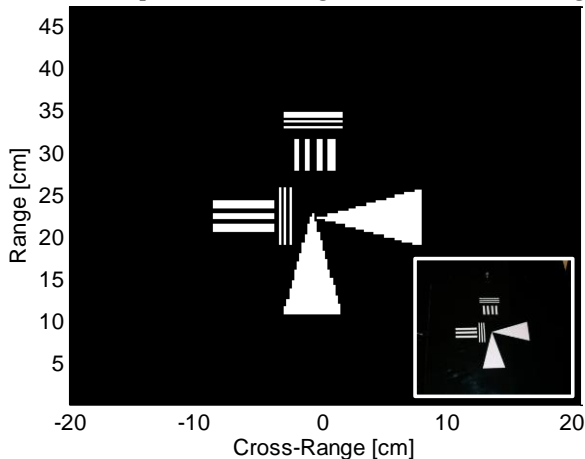

Figure 6 Target as constructed and then projected into the range – cross-range plane as in the final SAL image. The inset is a photograph of the real target.
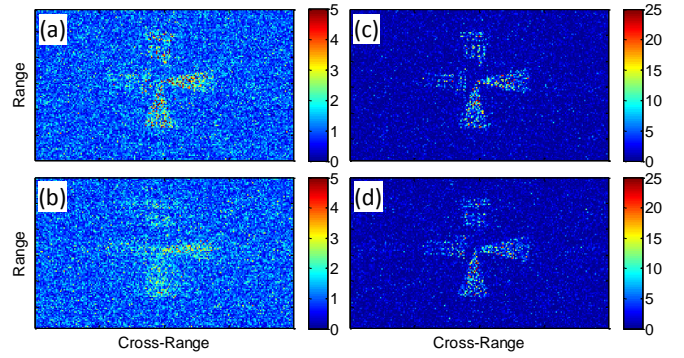
Figure 7 (a) The average of 5 independent 116x200 pixel SAL images with a mean of 1.1 photons per "on" pixel using a bright retro-reflector for phase correction or (b) PGA image (no retro) based phase error correction are shown. The color bars are normalized to the shot-noise background. (c,d) These SAL images are about 5 times higher transmit power and demonstrate marked improvement in the PGA corrected images. No averaging was applied to provide direct comparison with (a, b) at the same total image energy.

with >70% reflectivity and 32 degree incident angle the total expected received flux is approximately 650 photons/sec per mW of transmit power for the receive aperture of a single mode 10.5 µm diameter fiber 2 meters away. For 4 mW transmit power this corresponds to approximately 1 photon on average for every "on" pixel in the image, which includes a total collection time of 0.46 seconds for a 200 aperture position SAL collection. This photon budget was verified from the experimental collections.

To compare the performance and sensitivity of SAL imaging with and without image based phase correction such as PGA, a small index 2.0 ball retro reflector was alternately placed in the scene to provide a bright phase reference to estimate and correct the phase errors, or left out and PGA was applied to correct the phase errors. Several transmit powers were used and 500 independent SAL images were collected by setting an aperture motion of 0.75 mm using 200 steps. Each full aperture motion took > 40 seconds to complete owing to the slow step motion of the stage, therefore 10 range profiles were taken at each aperture position and the full aperture motion was repeated 50 times to collect the 500 images.

The images in Figure 7 represent the SAL images taken with and without the bright phase reference and at two power levels, approximately 1.1 and 5 photoelectrons per "on" pixel . The lower power images were averaged 5 times to make the image more visible. The colorbars to the right scale the image intensity in equivalent signal photoelectrons. The blurring in the PGA images at the lower transmit power is evident in Figure 7(b), however at the higher return level the image quality using PGA is visually indistinguishable from the one formed using the bright phase reference. Other things to notice are the strong speckle and the slight fading away from the center of the image due to the Gaussian beam profile.

To better quantify the performance of the SAL imaging at these low light levels and quantitatively compare the PGA

Figure 8 Estimated mutual information for the SAL imaging of the diffuse reference target. The red squares are data taken from a second run to fill in the high intensity data.

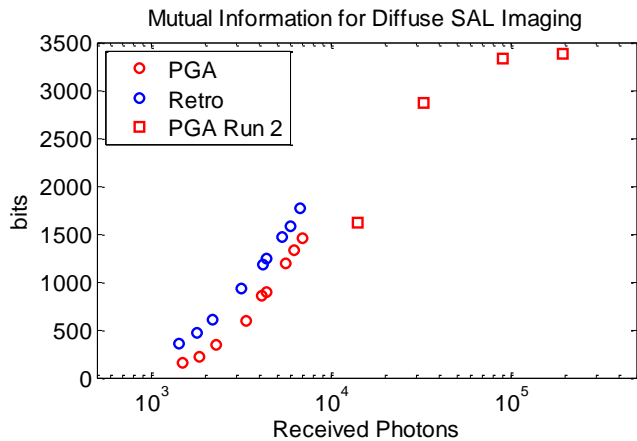images to the bright phase reference images, the 500 images under each condition were used to make estimates of the mutual information relative to the known target, Figure 6. Mutual information of images has found significant use in image processing for registration of disparate data [11,12]. The basis of these techniques are to use histograms of the pixel values in the images to estimate both the individual entropies $H(X)$ and $H(Y)$ and the joint entropy $H(X,Y)$ based on the pixel-wise 2D joint histogram. The mutual information is then calculated as $I(X;Y) = H(X) + H(Y) - H(X,Y)$. We use similar techniques here both to register and remove any residual cross-range shift of the individual images uncorrected by the PGA, and to calculate the mutual information for different power levels for quantitative comparison.

To provide good absolute measures of the mutual information, particularly for the PIE metrics, care had to be taken to avoid spuriously inflating the mutual information. Initially, as a reference image the average of the 500 SAL images at high power and with the phase reference was used. In this case, one could arbitrarily inflate the estimated mutual information by increasing the number of intensity bins used to generate the histograms. Taking a step back, a binary reference image generated by thresholding the averaged reference image was tried. Here too it was found that consistent mutual information values were difficult to obtain as one could vary result by changing the threshold value used to generate the binary image. In the end, the best consistency was enforced by using the binary image in Figure 6 as a reference. Even here a difficulty was that the size of the features in the reference image did not match the pixel size resulting in aliasing issues that provide an inconsistent number of "on" pixels in the reference image dependent on exact placement and down-sampling. However, by utilizing this binary reference image, consistent mutual information values were obtained even when the histogram bin number and size for the SAL images were varied by factors of two.

Figure 8 shows the results of the mutual information calculations as a function of the received number of photons. The SAL images phased with PGA show lower mutual information. Figure 9 summarizes the resulting PIE estimates calculated from the mutual information. The PIE is plotted as a function of the average measured

intensity of the "on" pixels. The total number of signal photons received is this average value multiplied by the number of "on" pixels in the binary image, which was 1292. The red squares are from a separate data set taken much later after an EDFA was added to the setup to boost the transmit power and help fill in the high intensity data.

These plots show clearly that although the SAL images for the two methods at the approximately 5 photon per pixel intensity are nearly indistinguishable in the images, the difference in the mutual information is measurable. A 20% reduction near the peak of the PIE curve is observed. Additionally, it shows that the mutual information and PIE falls off more rapidly at lower intensities for the PGA processed images than for the bright retro-reflecting phase referenced image. For comparison lines in Figure 9 are the theoretical values of PIE for target location as in Figure 1, except for the number of bins being 22 and 12.5 (average) respectively. The value of 22 was chosen as approximately the number of "off" bins for every "on" bin, and the value of 12.5 was chosen as a value that more closely matches the retro data and the high intensity PGA data. What we can see from these comparisons is that treating the SAL imaging problem as a number of separate target location tasks (i.e. find the location of a bright target among a zero background of 22 bins, repeat for every "on" pixel) gets us close to the measured value for this binary imaging result.

6. Discussion

The maximum mutual information for the binary reference image is 7865 bits. This is the value of the binary entropy function for the fraction of "on" pixels multiplied by the total number of pixels. It is also equivalent to the value given by Equation 6. This is much greater than the measured mutual information even at high intensity, which indicates that the speckle plays a significant role in lowering the mutual information. On a per pixel basis, this is approximately 6 bits per "on" pixel which means
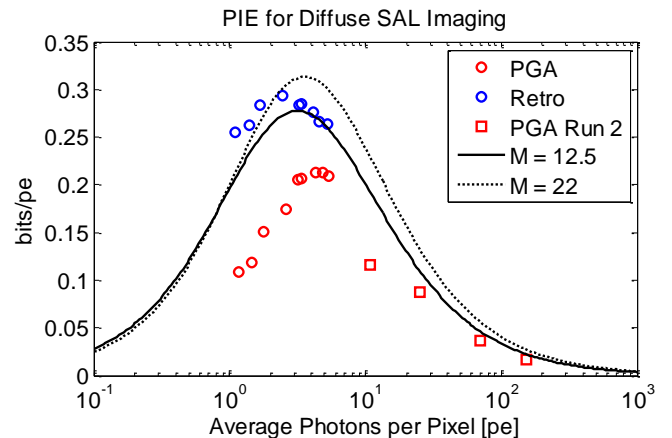
Figure 9 Estimates of the measured photon information efficiencies (PIE) for SAL imaging to a diffuse target as a function of the average return power per "on" pixel in the image. The blue circles are the PIE estimates for the SAL images phased using a retro-reflecting point target in the scene. (The signal power in the bright phase reference was removed from the images and the calculations.) The red circles and the red squares are the PIE estimates for the PGA corrected SAL images. The lines are the theoretical estimates of target location among M = 22 and 12.5 bins for speckled targets.

that at the peak PIE of 0.3 bits at ~4 photons only about 20% of the maximum information is collected, as compared to a little less than half the information at the high intensity PGA images. While this binary image information is probably the dominant form of the recoverable information, in general SAL images can have information contained in the image intensity and the image phase. An example of this extra information in the SAL data is the fact that the PGA algorithm is able to correct the phase errors due to the aperture motion. A quick estimate of the information needed to fully correct the large random phase errors (200 phases with resolution of $\pi/10$) gives $H_\phi = 200 \log_2(20) \cong 864$ bits, so we know that at least this amount of information is contained in the phase for well-focused images. As for intensity information, it can be expected that the speckle will have similar or worse degrading effects on the intensity information as it does on the binary image information.

We would also like to note that the coherent SAL images shown here are collected at very weak received photon flux – on the order 1 to 10 thousand photons per second. To make an average "on" pixel in the SAL images of Figure 7(a,b) a photon unit of energy was spread out over 200 independent chirped pulses each with 76.6 GHz of optical bandwidth, combining to total 0.46 seconds of coherent integration time. Additionally, due to the slow aperture motion, this energy actually took over 40 seconds to collect. To form an image, the energy had to be processed to end up in the correct pixel and do so coherently. For the 5 photon per pixel images in Figure 7(c,d), the initial SNR before cross-range compression is only 0.025. This is strong evidence that the PGA algorithm is very good at combining the information from the entire image to estimate the phase errors even when the signal from individual scattering points are buried in shot noise.

In conclusion, we have verified experimentally and through information metrics that the fundamental single photon sensitivity of coherent heterodyne measurements extends to SAL imaging. Coherent integration applies over the whole SAL aperture collection, and in the case of decoherence due to phase errors cause by the aperture collection, the coherent aperture can be recovered with image based correction algorithms such as the PGA at sub-photon per range measurement signal levels. While a loss of image information was observed with PGA it can be less than 20% as compared to images with a bright phase reference. While this work focuses on SAL using chirped FMCW ladar, most of the sensitivity conclusions should directly apply to other forms of coherent ladar.

References

1. K. W. Holman, D. G. Kocher, and S. Kaushik, "MIT/LL development of broadband linear frequency chirp for high resolution ladar," 65720J–65720J (2007).
2. N. Satyan, A. Vasilyev, G. Rakuljic, V. Leyva, and AmnonYariv, "Precise control of broadband frequency chirps using optoelectronic feedback," Opt. Express **17**, (2009).
3. P. A. Roos, R. R. Reibel, T. Berg, B. Kaylor, Z. W. Barber, and W. R. Babbitt, "Ultrabroadband optical chirp linearization for precision metrology applications," Opt. Lett. **34**, 3692 (2009).
4. S. M. Beck, J. R. Buck, W. F. Buell, R. P. Dickinson, D. A. Kozlowski, N. J. Marechal, and T. J. Wright, "Synthetic-aperture imaging laser radar: laboratory demonstration and signal processing," Appl. Opt. **44**, 7621–7629 (2005).
5. S. Crouch and Z. W. Barber, "Laboratory demonstrations of interferometric and spotlight synthetic aperture ladar techniques," Opt. Express **20**, 24237–24246 (2012).
6. L. Liu, "Coherent and incoherent synthetic-aperture imaging ladars and laboratory-space experimental demonstrations [Invited]," Appl. Opt. **52**, 579–599 (2013).
7. B. W. Krause, J. Buck, C. Ryan, D. Hwang, P. Kondratko, A. Malm, A. Gleason, and S. Ashby, "Synthetic aperture ladar flight demonstration," in *2011 Conference on Lasers and Electro-Optics (CLEO)* (IEEE, 2011), pp. 1–2.
8. Z. W. Barber, J. R. Dahl, T. L. Sharpe, and B. I. Erkmen, "Shot noise statistics and information theory of sensitivity limits in frequency-modulated continuous-wave ladar," J. Opt. Soc. Am. A **30**, 1335–1341 (2013).
9. J. W. Goodman, *Statistical Optics* (Wiley, 2000).
10. D. Zwillinger and Chemical Rubber Company, *CRC Standard Mathematical Tables and Formulae* (Chapman & Hall/CRC, 2003).
11. P. Viola and W. M. Wells,III, "Alignment by Maximization of Mutual Information," Int J Comput Vis. **24**, 137–154 (1997).
12. D. B. Russakoff, C. Tomasi, T. Rohlfing, and C. R. M. Jr, "Image Similarity Using Mutual Information of Regions," in *Computer Vision - ECCV 2004*, T. Pajdla and J. Matas, eds., Lecture Notes in Computer Science No. 3023 (Springer Berlin Heidelberg, 2004), pp. 596–607.

Appendix 2) SPIE Proceedings article on CLR method.

Multi-target compressive laser ranging

Pushkar P. Pandit, Jason R. Dahl, Zeb W. Barber, W. Randall Babbitt

Spectrum Lab, Montana State University, Bozeman, Montana, USA 59717

ABSTRACT

Compressive laser ranging (CLR) is a method that exploits the sparsity available in the range domain using compressive sensing methods to directly obtain range domain information. Conventional ranging methods are marred by requirements of high bandwidth analog detection which includes severe SNR fall off with bandwidth in analog-to-digital conversion (ADC). Compressive laser ranging solves this problem by obtaining sub-centimeter resolution while using low bandwidth detection. High rate digital pulse pattern generators and off the shelf photonic devices are used to modulate the transmitted and received light from a superluminescent diode. CLR detection is demonstrated using low bandwidth, high dynamic range detectors along with photon counting techniques. The use of an incoherent source eliminates speckle issues and enables simplified CLR methods to get multi-target range profiles with 1-3cm resolution. Using compressive sensing methods CLR allows direct range measurements in the sub-Nyquist regime while reducing system resources, in particular the need for high bandwidth ADC.

Keywords: Compressive sensing, laser ranging, ladar, lidar

1. INTRODUCTION

Conventional laser ranging (LiDAR, LADAR) generally requires high bandwidth detectors and analog-to-digital converters (ADCs) which face severe SNR penalty with increasing bandwidth. Compressive sensing (CS) as a measurement method is gaining momentum, particularly in hardware or resource constrained sensing to work around such requirements[1]. Compressive sensing leverages the sparsity found in most real-world scenes, to enable unconventional measurement modalities with the potential to use measurement resources more efficiently. Laser ranging should be highly amendable to a compressive sensing methodology since often the range scene consists of limited number of targets. In particular, in hard target ranging only a single return is measured due to the opacity of most solid materials.

Despite the sparsity found in the range domain, direct application of CS techniques for time-of-flight ranging is hindered by the fact that the ranging measurement method of impinging the scene with a pulse of radiation and collecting the return is at heart a convolution measurement rather than an integrative projective measurement that can be expressed as an inner product. In 2011 (Babbitt et al.)[2] we proposed an interpretation, Compressive Laser Ranging (CLR), that casts all time-of-flight of ranging methods fundamentally as projective measurements of receive waveforms with the convolution product of a transmit waveform and the object. We then recast the measurements, by proper reordering of the products, as an inner product of the object vector against basis vectors that represent the correlation of the transmit and receive waveforms. This recasting allows one to apply compressive sampling techniques directly in the sparse range domain utilizing modulation on both transmit and receive paths followed by slow integrated measurement of the optical intensity.

In particular, we proposed the use of pseudorandom binary modulation on both transmit and receive optical paths that efficiently utilizes both the CW transmit power and the return energy and can be implemented using standard telecommunications equipment. The advantage of this approach is that only low bandwidth optical detection and ADC's are required. In Babbitt et al., we presented a proof-of-concept demonstration of this technique at 1 GHz bit rate. However, that demonstration was limited to only single targets due to time varying, multi-reflection interference and laser speckle, which hurt the stability of the integrated projective measurements. In this work, we demonstrate the simultaneous measurement of multiple targets with CLR with the use of a low temporal coherence superluminescent diode as a source and increase the bit rate (bandwidth) of our CLR demonstration. Additionally, we demonstrate CLR utilizing photon counting with a Geiger Mode Avalanche Photodiode (GM-APD) to demonstrate high sensitivity at 10 Gigabit per second (Gbps) modulation rates.

2. THEORY

While CS is a rapidly evolving field in signal processing and measurement theory, we begin here with some very basic background theory to introduce the simple modifications we use to accomplish CLR. The key insight of CS[3] is that prior knowledge of a signal's sparsity S (number of non-zero elements in the object vector that represents the signal in some basis) can be used to design measurements that allow accurate reconstructions with significantly less measurements than is conventionally required. In particular, CS techniques do not require the sparse features in a basis be known, or even that the sparsifying basis is known before measurement, as long as the sampling matrix that represents the measurement fulfills certain properties such as the Restricted Isometry Property (RIP)[4].

The basic CS theory goes as follows: Consider a sparse signal X of length N. The signal X can be reconstructed by taking M measurements ($M < N$) of the inner product of the signal X against a set of known basis vectors A_m. Expressed in matrix form, $Y = AX$. The linear equation is an underdetermined system which has many solutions. The goal of CS is to find a sparse solution that best represents the signal, also known as L0 minimization. There are several approaches to solving this problem including convex optimization[5], basis pursuit[6], and combinations[7,8]. Greedy basis pursuit algorithms such as CoSaMP (Compressive Sampling Matching Pursuit)[9] and OMP (Orthogonal Matching Pursuit)[10] are fairly popular due to their low computational complexity and relative robustness in reconstructing the signal X provided sufficient measurements are made. The number of measurements required is typically $M > O(S \log(N))$ for $S << N$, it can be seen that for sparse signals M is much less than N. CS has been widely explored for 2D imaging techniques where the scene is measured using a sampling matrix consisting of pseudorandom binary patterns[11,12].

The innovation in Compressive Laser Ranging (CLR) is the recasting of time-of-flight measurements from a convolution measurement to an inner product measurement, allowing CS techniques to be directly applied in the generally sparse time-of-flight basis. In the approach presented here, the signal is a range profile $R(\tau)$, which represents the reflectivity of a 1D scene of targets as a function of round-trip delay τ. The transmitted signal and the received signal are temporally modulated and collected using a an integrating detector, which allows for $R(\tau)$ to be determined without the need for a time-domain signal. The transmitted signal is optically modulated by a signal $Tx_m(t)$ and the return signal is optically modulated by a signal $Rx_m(t)$ before reaching a detector which measures the total energy received. This process is repeated with different Tx and Rx modulations to produce M measurements ($m = 1,…, M$). In order to directly apply CS basis pursuit algorithms to reconstruct the range profile, we have to represent these measurements with a sampling matrix. The description and physical explanation for this sampling matrix is given below. We begin with a temporally modulated transmitted signal $Tx_m(t)$. This transmitted signal reflects off the targets represented by the range profile $R(\tau)$ forming a convolution product given as :

$$I_m(t) = \int_{-\infty}^{\infty} Tx_m(t - \tau)R(\tau)\, d\tau$$

$I_m(t)$ represents the return signal before the receive modulator, which is then temporally modulated by $Rx_m(t)$. After modulation the signal is temporally integrated with a detector. Each of the integrated measurements in the measurement vector Y are given by:

$$Y_m = \int_{-\infty}^{\infty} Rx_m(t)I_m(t)\, dt$$

Substituting the value for I_m and rearranging gives and inner product measurement in the delay domain:

$$Y_m = \int_{-\infty}^{\infty} R(\tau)D_m(\tau)\, dt$$

Where $D_m(\tau)$ is a function representing the correlation product of the transmit and receive modulations,

$$D_m(\tau) = \int\limits_{-\infty}^{\infty} Tx_m(t)Rx_m(t+\tau)\,dt$$

If we discretize the measurement problem, the CLR sensing function and the range profile can be represented respectively as a mixing matrix D of dimensions M x N as $D_{mn} = D_m(n\delta\tau + \tau_H)$ and a sparse signal vector $R_n = R(n\delta\tau + \tau_R)$. Where τ_R is the average round trip delay to the targets and τ_H is the delay required to accurately overlap the $Rx_m(t)$ signal with the return signal since inherent delays are caused by fibers and electronics in the system. B_{TR} is the bandwidth of the signals $Tx_m(t)$ and $Rx_m(t)$, which defines $\delta\tau = \frac{1}{B_{TR}}$. The problem therefore is to solve for R in $Y = DR$. CS recovery algorithms such as CoSaMP and OMP can then be used to reconstruct the range profile.

The CLR range resolution is given by $dR = c/(2B_{TR})$ where c is the speed of light. The bandwidth of the detector and ADCs required in this case is B_{TR}/N which is orders of magnitude lower than that required for high resolution incoherent ranging systems given by $c/(2dR)$. The range window for CLR is approximately the sum of the widths of $Tx_m(t)$ and $Rx_m(t)$ given by $N\delta\tau$ and is weighted by their correlation with a full width at half maximum (FWHM) of about $N\delta\tau/2$.

3.   DEMONSTRATION OF MULTI-TARGET CLR

The CLR experiments published in Babbitt et al. were revisited to demonstrate ranging to multiple simultaneous targets. The CLR demonstrator used was very similar to the previous experiments with a few slight changes. Most significantly, the laser source was changed to a very low temporal coherence superluminescent diode in place of the Fabry-Perot diode laser. The low coherence source completely eliminated partial coherence issues from multiple-reflections and laser speckle that plagued our earlier work and prevented the demonstration of multi-target ranging. To provide multiple targets along a single line of sight, partially reflecting mirrors (PRM) were included as targets along the line of sight. Additionally, highly reflecting mirrors were included that could be taken in and out of the path using "flipper" mirror mounts. A final change was that a Tektronix AWG 610 arbitrary waveform generator (AWG) was utilized that allowed an increase of the bit rate up to 2.5 Gbps.
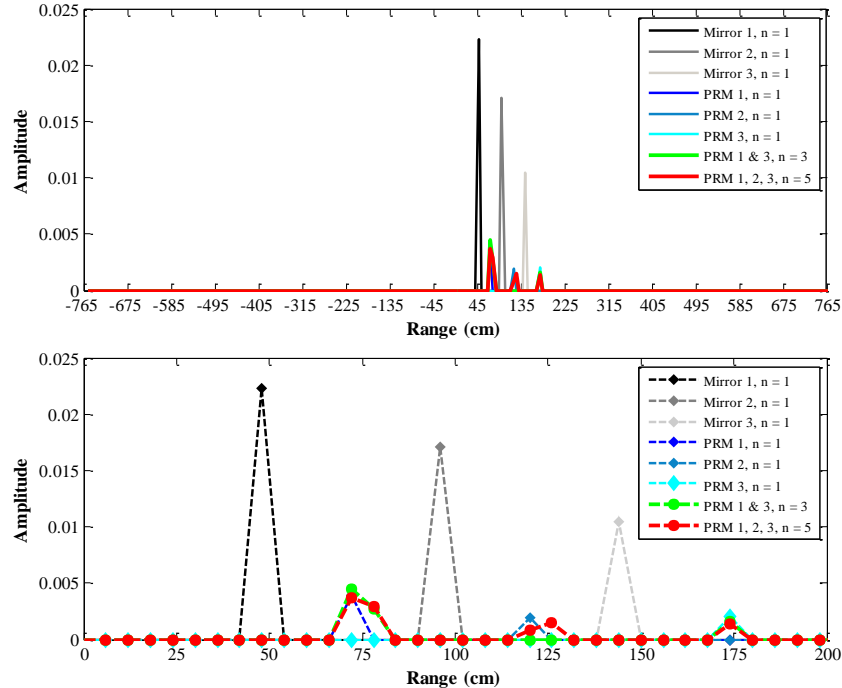

Figure 1. The range profiles for six target positions determined using the CoSaMP algorithm. A) Shows the whole range profile. B) Zoomed in on the range peaks. The black/grey profiles are for the mirrors set at 48 cm, 96 cm, and 144 cm. The blue, red, and green profiles are for the partially reflecting mirrors (PRM) set at 72 cm, 120 cm, and 168 cm.

For this demonstration each pair of waveforms (transmit and receive) contains two 2.5 gigabits per second (Gbps) pseudo-random sequences produced by the arbitrary waveform generator's (AWG) marker ports. The output voltage of the marker's was set to 0 V for the low level and 2.5 V for the high. For the experiment, sub-measurements were created by repeating the transmit waveform, but alternating the receive binary waveform with its complement. The output of the detector was then mixed with a square waveform from the AWG that is synchronized with the receive waveform and flips the sign of the second measurement. The output of the mixer is a dual polarity signal that when low pass filtered (integrated over the two sub-measurements) has the background level automatically removed. We found that this process improves the conditioning of the measurement matrix and makes the CLR results more stable. The low pass filtered measurement is captured with a 40 ksps, 14-bit ADC. After collection of the signal level for one pair of waveforms, the next pair of waveforms was loaded onto the AWG and the measurement was repeated.

The binary waveforms for this experiment were 128-bits long with 30 pairs of waveforms used. The measurements for all six targets were processed with a CoSaMP[13] and OMP[14] algorithms that yielded the locations and amplitudes for the targets. Figure 1 is a plot of the range profile for the mirrors and PRM using the CoSaMP algorithm.

Figure 2 is the range profiles for the same targets in Figure 1 but used the OMP algorithm to process the data. For both algorithms the range bins are 6 cm apart.
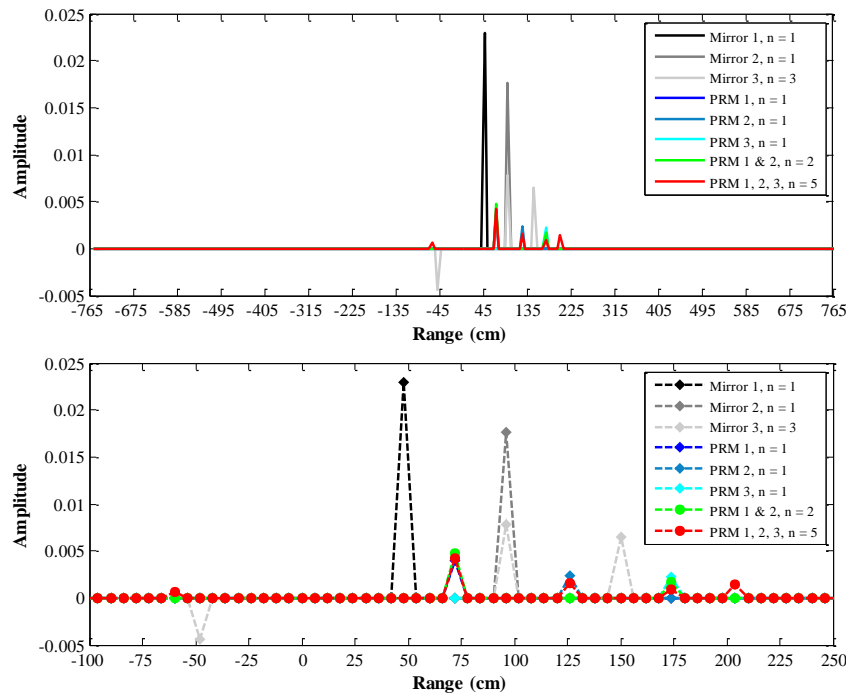

Figure 2. The range profiles for six target positions determined using the OMP algorithm. A) Shows the whole range profile and B) is zoomed in on the range peaks. The black/grey profiles are for the mirrors set at 48 cm, 96 cm, and 144 cm. The blue, red, and green profiles are for the partially reflecting mirrors (PRM) set at 72 cm, 120 cm, and 168 cm.

The black/grey (high reflecting mirrors) and blue (PRM) profiles were ranged one at a time with 30 measurements then processed. The CoSaMP for the single mirrors was set to find one target (n=1) each time while the OMP had to be set to search for three targets (n=3) for the farthest away mirror. The green profile is the first and third PRM ranged at the same time with the same 30 measurements. The CoSaMP for this measurement was set to find three targets (n=3) while the OMP was set to find two targets (n=2). The red profile is all three PRM ranged at the same time with the CoSaMP set to find five targets (n=5) and the OMP set to find five targets (n=5).

Both of the algorithms tested were able to find the target locations, but the accuracy and reliability varies between them. The CoSaMP from these tests seemed to perform more reliably then did the OMP. In Figure 2 the third mirror has other

target locations showing up at mirror two and one negative target at -50 cm. A similar error occurred for the red profile where all three PRM were ranged at the same time. In this case extra targets were found beyond the third PRM and at -60 cm. The accuracy for the ranges also depends on the placement of the objects. If an object is located in-between range bins then the algorithm has a harder time positioning it correctly.

4. CLR DEMONSTRATION AT 10 GBPS WITH PHOTON COUNTING DETECTORS

4.1 Experimental Setup

The next demonstrations of the CLR method consisted of increasing the bitrate of the modulating waveforms to 10 Gbps and exploring the use of photon counting detectors to better understand the fundamental sensitivity of the method. To increase the bitrate we switched the waveform generation system to utilize two 12.5 Gbps Advantest D3186 pulse pattern generators (PPG's). The PPGs were time synched by driving the 10 MHz reference from one PPG into a DDS based function generator, which can be detuned slightly to cause a slow temporal drift in the timing. The relative timing is then monitored on an oscilloscope and the detuning is set to zero when the two PPGs are time synched. We are in the process of replacing the PPGs for waveform generation with fast digital transceiver ports from an FPGA, with the ultimate goal to have all the processing implemented on FPGA to demonstrate the capability to make the CLR system into a compact laser ranging system.
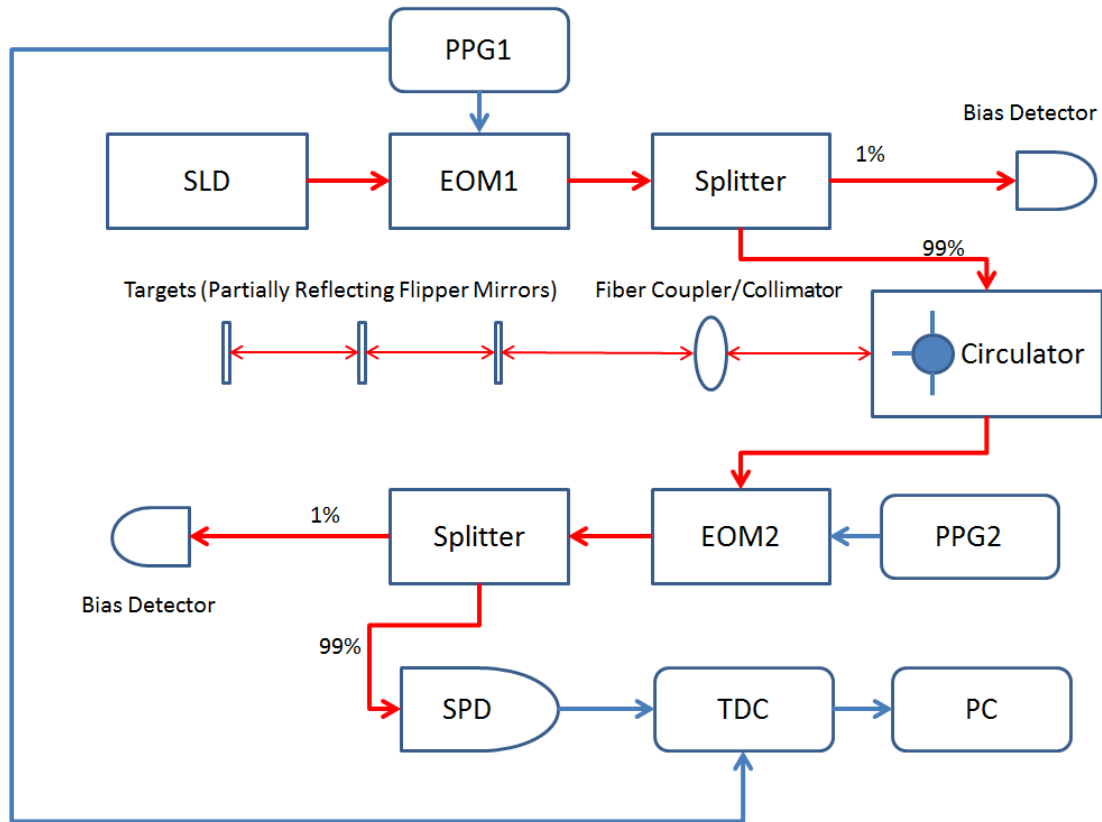

Figure 3. The Compressive Laser Ranging Setup. Light from an incoherent source is modulated by EOMs with binary waveforms from the PPGs. Return signal from the target (flipper mirrors) is collected using a single photon detector and digitized for processing with a PC.

To explore the fundamental sensitivity of the CLR, in these experiments we utilized an ID Quantique 220 GM-APD as a detector. This detector operates in a free-running mode and has adjustable photon detection efficiency and dead-time which affect the dark-count rate of the detector. For the experiments here the detector was operated at 10% detection efficiency and 1 μs dead-time, which results in about 2 kHz dark count rate. The photon count pulses out of the detector were time tagged using a Time-to-Digital Converter (TDC) (Surface Concept SC-TDC-1000/08 S). Due to the discrete nature and time based measurement of the photon counts, we changed the experimental design to remove the analog

mixer and low pass filter and produced the dual polarity signal by subtracting the alternate waveforms in post processing. As part of the change, we changed the measurement process from completing the measurement with one pair of waveforms before moving on to the next, to one in which the whole measurement sampling matrix is sampled before repetition to generate photon counting statistics for the measurement.

An illustration of the experimental setup used for the GM-APD based measurements is shown in Figure 3. The incoherent illumination source SLD is a 1550nm superluminescent diode with a FWHM bandwidth of about 50 nm. The light from the diode is modulated by a null biased electro-optic intensity modulator EOM1 for which the transmit patterns $Tx_m(t)$ are generated by the pulse pattern generator PPG1. The 1% output from a 99:1 splitter after EOM1 is used to monitor and adjust the null bias of EOM1. The 99% output of the splitter is sent through a circulator to a fiber collimator/coupler, which creates a free space beam. The light hits targets which are partially reflecting flipper mirrors and returns to the circulator via the fiber coupler/collimator. The output from the circulator is passed to a second null biased electro-optic intensity modulator EOM2 for which the return patterns $Rx_m(t)$ are generated by the second pulse pattern generator PPG2. The light from EOM2 is again passed to through the 99% end of a 99:1 splitter where the light from EOM2 is massively attenuated (80 dB) and collected by single-photon detector (SPD). The detector output is then sampled by the TDC for time digitization. The 1% is again used to monitor and adjust the null bias of EOM2. The TDC uses a trigger from PPG1 in order to synchronize the received photon counts with the beginning of the waveforms transmitted to EOM1 and EOM2. The digitized data is sent to a PC which does further processing. Photon counts from multiple waveform pairs being sent to EOM1 and EOM2 are processed in order to obtain the measurements Y.

The flipper mirror targets were spaced ~48 cm from each other and the flippers were used in order to range the targets individually to verify the range at each of the target locations. In order for the system to work, the patterns sent to the EOMs need to overlap in the right order. To synchronize the patterns a delay needs to be set on the second PPG in order to compensate for the delay from the electronic cables and fiber components which was defined above as τ_H. In order to calculate the delay, a single 10 ns pulse is transmitted to both the EOMs with the PPGs synchronized. The measured time output from the SPD can be observed real time on the PC, by adjusting the delay on the PPGs such that both the pulses overlap the highest signal and the delay τ_H is obtained.

The results presented here were obtained at two different resolutions by changing the data rates of the PPGs (5 Gbps and 10 Gbps) to demonstrate resolutions of 3 cm and 1.5 cm respectively. Pseudorandom binary waveforms were created using MATLAB and uploaded to the PPGs and saved for further processing. The bitrates were chosen to ensure good fidelity of the binary waveforms and the EOMs binary low levels were set to 0 V and binary high levels were set to 5 V. The modulation was thus positive definite, which means that the waveforms sent to the targets were binary 0s and 1s. The pseudorandom patterns in the waveform were separated by a certain number of zeroes in order to make each pattern in the waveform distinguishable while observing the SPD data and during processing of the data. In order to compensate for high bias from these positive definite signals and to reduce background noise the dual polarity approach was used. Here each measurement consists of two sub-measurements, one using Tx_m and Rx_m and a second using Tx_m and $1 - Rx_m$. The TDC captures the photon count data of both these sub-measurements to form the measurements Y. The measurements were then processed using CoSaMP along with the saved pseudorandom patterns from which the correlation based sampling matrix D described above was constructed.

4.2 Results and Discussion

Pattern lengths of 128 bits were chosen for the setup with both 1.5 cm and 3 cm resolution. The number of measurements, M, was 30 which is much less than N which for 128 bit patterns is 255. It is however greater than $S\log(2N)$ which is ~19 for S = 3, the number of targets. The data collected from the TDC is processed so that the number of photon counts corresponding to each of the 30 patterns to yield the measurements Y to be used with CS recovery algorithms. For the data below the total number of photon counts for all 30 measurements was approximately 60,000. The measurements for the scene were processed with a CoSaMP algorithm, which yielded the results for 3 cm and 1.5 cm resolution. All 3 targets were simultaneously measured for 3 cm setup and a range profile is shown in Figure 4.
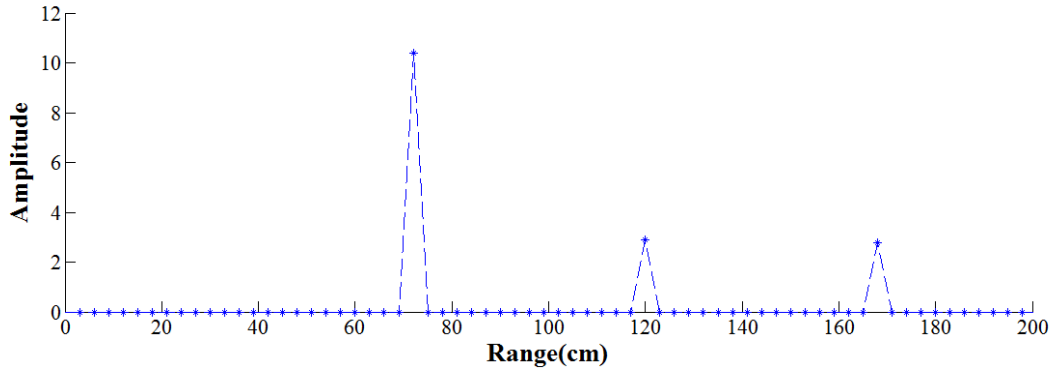
Figure 4. CLR range measurements using 5 Gbps waveforms which give a resolution of 3cm. The location of three targets were located simultaneously.

The range profiles for waveforms at 10 Gbps, which yield a resolution of 1.5 cm are shown in Figure 5. To simulate a changing scene two targets were ranged with one being stationary as a reference range source. For the higher resolution system the number of measurements was increased from 30 to 60, however it is still much smaller than the scene of length 255.
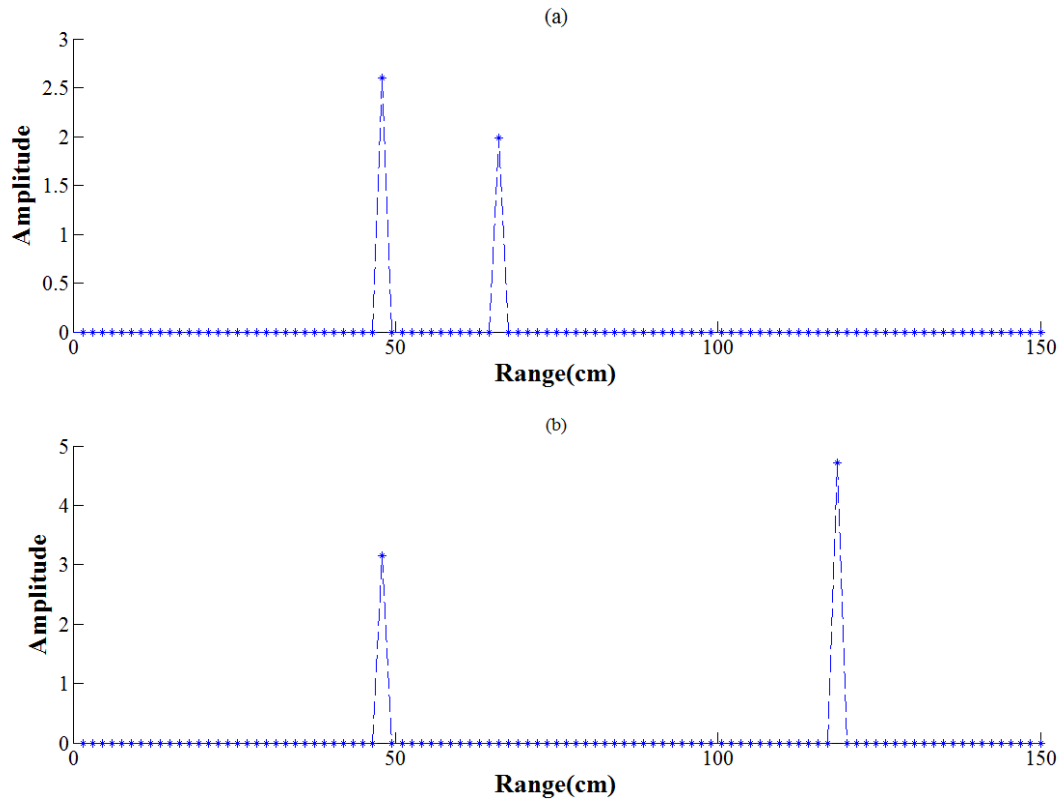

Figure 5. CLR range profile for 1.5 cm resolution setup. (a) Second target 20 cm from the reference target (b) Second target ~60 cm from the reference target.

Compressive laser ranging is able to achieve high resolution range profiles with multiple targets without the need for high bandwidth detectors or ADCs. The GM-APD has high timing resolution of ~200 ps, which means the 10 Gbps ranging presented here represents a factor of two increase in range resolution, however this resolution could be retained for much slower detectors. Due to the availability of relatively cheap and compact electronics, which can produce multi-

gigabit pseudorandom binary waveforms it is possible to create a compact and efficient high resolution ranging system. By increasing the data rate and bit length it is possible to create a higher resolution and a larger window for ranging.

In summary, the CLR method was demonstrated with range profiles consisting of multiple targets by use of a low coherence superluminescent diode to eliminate uncontrolled coherence and laser speckle effects. Additionally, using CS methods circumvents the requirement for high bandwidth detectors and ADCs. This approach only requires high bandwidth binary modulation and low bandwidth detection to range scenes with sparse profiles. CLR could be a promising technique for ranging where low peak transmit power levels are required and detector and ADC bandwidth is limited.

REFERENCES

[1] Adcock, B., Hansen, A. C.., Roman, B., "The quest for optimal sampling: Computationally efficient, structure-exploiting measurements for compressed sensing," ArXiv Prepr. ArXiv14036540 (2014).
[2] Babbitt, W. R., Barber, Z. W.., Renner, C., "Compressive laser ranging," Opt. Lett. **36**(24), 4794–4796 (2011).
[3] Baraniuk, R. G., "Compressive sensing [lecture notes]," Signal Process. Mag. IEEE **24**(4), 118–121 (2007).
[4] Candes, E. J., "The restricted isometry property and its implications for compressed sensing," Comptes Rendus Math. **346**(9), 589–592 (2008).
[5] Rudelson, M.., Vershynin, R., "Sparse reconstruction by convex relaxation: Fourier and Gaussian measurements," Inf. Sci. Syst. 2006 40th Annu. Conf. On, 207–212, IEEE (2006).
[6] Chen, S. S., Donoho, D. L.., Saunders, M. A., "Atomic decomposition by basis pursuit," SIAM J. Sci. Comput. **20**(1), 33–61 (1998).
[7] Donoho, D. L., "Compressed sensing," IEEE Trans. Inf. Theory **52**(4), 1289–1306 (April).
[8] Figueiredo, M. A., Nowak, R. D.., Wright, S. J., "Gradient projection for sparse reconstruction: Application to compressed sensing and other inverse problems," Sel. Top. Signal Process. IEEE J. Of **1**(4), 586–597 (2007).
[9] Needell, D.., Tropp, J. A., "CoSaMP: Iterative signal recovery from incomplete and inaccurate samples," Appl. Comput. Harmon. Anal. **26**(3), 301–321 (2009).
[10] Tropp, J.., Gilbert, A. C., Signal recovery from partial information via orthogonal matching pursuit, Apr (2005).
[11] G. A. Howland, P. B. D.., J. C. Howell., "Photon-counting compressive sensing laser radar for 3D imaging," Appl. Opt. **50**(31), 5917 (2011).
[12] Duarte, M. F., Davenport, M. A., Takhar, D., Laska, J. N., Sun, T., Kelly, K. F.., Baraniuk, R. G., "Single-pixel imaging via compressive sampling," IEEE Signal Process. Mag. **2008**.
[13] Needell, D.., Tropp, J., "CoSaMP: Iterative signal recovery from incomplete and inaccurate samples."
[14] Tropp, J. A., Laska, J. N., Duarte, M. F., Romberg, J. K.., Baraniuk, R. G., "Beyond Nyquist: Efficient Sampling of Sparse Bandlimited Signals," IEEE Trans. Inf. Theory **56**(1), 520–544 (2010).
[15] Howland, G. A., Lum, D. J., Ware, M. R.., Howell, J. C., "Photon counting compressive depth mapping," Opt. Express **21**(20), 23822–23837 (2013).
[16] Baraniuk, R.., Steeghs, P., "Compressive radar imaging," Radar Conf. 2007 IEEE, 128–133, IEEE (2007).
[17] Tello Alonso, M., López-Dekker, P.., Mallorquí, J. J., "A novel strategy for radar imaging based on compressive sensing," Geosci. Remote Sens. IEEE Trans. On **48**(12), 4285–4295 (2010).